Article

Cell Reports

# Heterogeneities in *Nanog* Expression Drive Stable Commitment to Pluripotency in the Mouse Blastocyst

## Graphical Abstract

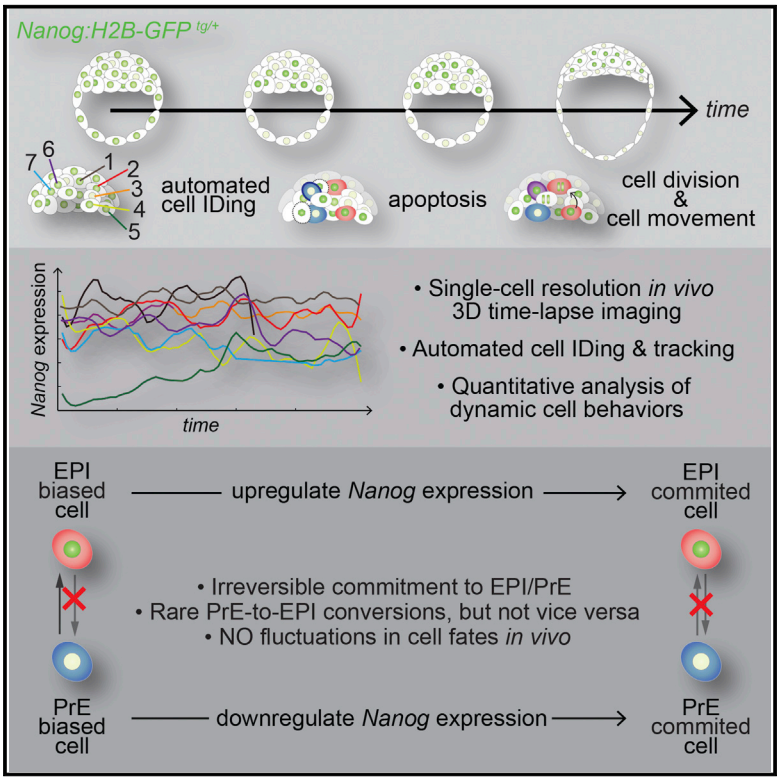


## Highlights

- Single-cell resolution live imaging of the pluripotent EPI lineage in vivo
- Fluctuations between distinct developmental states are not observed in vivo
- Occasionally, cells can change their fate toward a pluripotent identity
- Rapid expansion of the pluripotent lineage once specified

## Authors

Panagiotis Xenopoulos, Minjung Kang, ..., Stefano Di Talia, Anna-Katerina Hadjantonakis

## Correspondence

hadj@mskcc.org

## In Brief

Xenopoulos et al. use high-resolution live cell imaging to visualize the emergence of the pluripotent lineage in mammalian embryos. Automated quantitative single-cell image analysis reveals that distinct developmental states are not observed to fluctuate in the mouse embryo. Occasionally, cells can change their fate toward a pluripotent identity, which once specified is rapidly expanded.

Xenopoulos et al., 2015, Cell Reports *10*, 1508–1520
March 10, 2015 
http://dx.doi.org/10.1016/j.celrep.2015.02.010

OPEN ACCESS
CellPress

Cell Reports
Article

# Heterogeneities in *Nanog* Expression Drive Stable Commitment to Pluripotency in the Mouse Blastocyst

Panagiotis Xenopoulos,[1,5] Minjung Kang,[1,2,5] Alberto Puliafito,[3] Stefano Di Talia,[4] and Anna-Katerina Hadjantonakis[1,*]
[1]Developmental Biology Program, Sloan Kettering Institute, New York, NY 10065, USA
[2]Biochemistry, Cell and Molecular Biology Program, Weill Graduate School of Medical Sciences of Cornell University, New York, NY 10065, USA
[3]Laboratory of Cell Migration, Candiolo Cancer Institute - FPO, IRCCS, Candiolo, Torino 10060, Italy
[4]Department of Cell Biology, Duke University Medical Center, Durham, NC 27710, USA
[5]Co-first author
*Correspondence: hadj@mskcc.org
http://dx.doi.org/10.1016/j.celrep.2015.02.010


## SUMMARY

**The pluripotent epiblast (EPI) is the founder tissue of almost all somatic cells. EPI and primitive endoderm (PrE) progenitors arise from the inner cell mass (ICM) of the blastocyst-stage embryo. The EPI lineage is distinctly identified by its expression of pluripotency-associated factors. Many of these factors have been reported to exhibit dynamic fluctuations of expression in embryonic stem cell cultures. Whether these fluctuations correlating with ICM fate choice occur in vivo remains an open question. Using single-cell resolution quantitative imaging of a *Nanog* transcriptional reporter, we noted an irreversible commitment to EPI/PrE lineages in vivo. A period of apoptosis occurred concomitantly with ICM cell-fate choice, followed by a burst of EPI-specific cell proliferation. Transitions were occasionally observed from PrE-to-EPI, but not vice versa, suggesting that they might be regulated and not stochastic. We propose that the rapid timescale of early mammalian embryonic development prevents fluctuations in cell fate.**

## INTRODUCTION

Pluripotency is defined as the ability of a cell to differentiate and give rise to all somatic and germ cells (Nichols and Smith, 2012). Although pluripotency can be induced in differentiated cells (Takahashi and Yamanaka, 2006), how a pluripotent population emerges in its native context, within the early mammalian embryo, remains an open question. Insight will come from elucidating the dynamic cell behaviors and molecular mechanisms underlying the development of the mammalian blastocyst, the embryonic stage at which a bona fide pluripotent population—the epiblast (EPI)—is established.

The EPI is molecularly distinct and spatially segregated from the two extra-embryonic lineages, the primitive endoderm (PrE) and trophectoderm (TE) of the mouse blastocyst. The specification of these lineages occurs as two sequential binary cell-fate decisions. The first involves specification and segregation of TE from inner cell mass (ICM), while the second occurs within the ICM and involves the specification of EPI and PrE precursors, and their eventual segregation into adjacent tissue layers (reviewed in Schrode et al., 2013). By late blastocyst stage, the EPI and PrE lineages are defined both by their position within the embryo and expression of lineage-specific transcription factors, such as NANOG in the EPI, and GATA6 and GATA4 in the PrE (Xenopoulos et al., 2012). Recent studies have illustrated that EPI/PrE allocation occurs in at least three successive steps (Chazaud et al., 2006; Frankenberg et al., 2011; Plusa et al., 2008). Initially, lineage-specific transcription factors, such as NANOG and GATA6, are co-expressed by all ICM cells, suggesting a multi-lineage priming state. Thereafter, NANOG and PrE lineage-specific transcription factors exhibit mutually exclusive expression, as lineage progenitors emerge in a salt-and-pepper distribution within the ICM. At this stage, GATA4 becomes activated in PrE progenitors, concomitant with NANOG downregulation. Finally, lineage segregation is achieved with the localization of PrE cells to the surface of the ICM. At this time, other pluripotency-associated factors become restricted to EPI cells, which have become positioned internally within the ICM. Notably, NANOG is one of the first markers to be restricted within the EPI, whereas OCT4 and SOX2 become subsequently downregulated in PrE progenitors and restricted to EPI progenitors.

The initial specification of EPI and PrE progenitors appears to occur in a spatially random manner (Schrode et al., 2014) and could be achieved if a stochastic process were to underlie this second fate decision. Indeed, an analysis of transcriptomes of single ICM cells revealed that gene expression is highly heterogeneous at earlier stages, exhibiting no apparent lineage specificity and a hierarchical relationship of marker expression only appearing in the late blastocyst (Guo et al., 2010; Kurimoto et al., 2006; Ohnishi et al., 2014).

A degree of heterogeneity has been observed at both protein and mRNA level for various pluripotency-associated factors in embryonic stem cell (ESC) cultures. Many studies have focused

on *Nanog*, a central component of the core pluripotency transcriptional network (Chambers et al., 2007; Kalmar et al., 2009). Experiments in ESCs have suggested that *Nanog* expression displays dynamic fluctuations that may correlate with a cell's fate choice between self-renewal and differentiation. However, it is unclear whether fluctuations in gene expression take place in vivo in embryos where cell differentiation occurs on a shorter timescale, nor whether they predict fate choice or fate reversion. Notably, understanding how pluripotent cells behave in embryos may provide information that can be reconciled with observations made in ESCs (Smith, 2013).

To determine how the EPI emerges within the mouse blastocyst, we generated a reporter of *Nanog* transcription (*Nanog:H2B-GFP*). Derivation of ESCs from reporter-expressing embryos revealed heterogeneous gene expression as an adaptation to ESC propagation. Using live imaging, we quantified the dynamics of *Nanog* expression in individual cells of live blastocysts, establishing how *Nanog* expression influences the fate of ICM cells. By contrast to ESCs maintained in culture, fluctuations in *Nanog* expression between distinct developmental states did not, generally, occur in vivo. However, we noted rare cases of cells unidirectionally switching their fate, from a PrE to EPI identity. Since ICM fate changes were only observed toward the EPI, and not toward PrE, we concluded that this change was not stochastic. Our analyses also revealed events of selective apoptosis at the onset of ICM lineage differentiation, followed by a burst of cell proliferation in EPI-committed cells. Collectively, these data suggest that, although it may be dynamic in ESCs, the emergence of a pluripotent identity is sequential and linear in vivo and not accommodating reversibility in fate. In this way, after its allocation, the pluripotent cell population might be protected, thereby ensuring the development of somatic lineages.

## RESULTS

### BAC-Based *Nanog* Transcriptional Reporters Mark the Pluripotent State in ESCs and Embryos

To probe the dynamics of the pluripotent state, we developed a BAC-based *Nanog* transgenic transcriptional reporter, based on a previous design used as a readout of cellular reprogramming during iPS cell generation (Okita et al., 2007) (Figure S1H). For single-cell resolution readouts of *Nanog* expression, we generated nuclear-localized human histone H2B fusion versions of the reporter (Figures 1A, 1C, and S1E).

To validate transgene activity, we analyzed reporter expression in transgenic ESCs under various culture conditions. These conditions included the presence or absence of leukemia inhibitory factor (LIF), and 2i+LIF, which promote the self-renewal of ESCs, induce differentiation, or ground state pluripotency, respectively (Ying et al., 2008). Immunostaining of ESCs in 2i+LIF or serum-LIF conditions revealed markedly increased or decreased expression, respectively, of both reporter and NANOG protein. Heterogeneous but correlated GFP and NANOG expression was observed in *Nanog:GFP*$^{Tg/+}$ and *Nanog:H2B-GFP*$^{Tg/+}$ ESCs maintained in serum+LIF conditions (Figures 1A, 1B, S1D, and S1E). Single-cell quantitative image analyses of immunostained *Nanog:H2B-GFP*$^{Tg/+}$ ESCs maintained under different conditions further validated reporter efficacy (Figures 1B, S1E, and S1F). Moreover, we observed an increased correlation of reporter activity with NANOG protein for the *Nanog:H2B-GFP* transgene, compared to the targeted *Nanog* transcriptional reporter in the heterozygous TNGA ESCs (Chambers et al., 2007) (Figures S1E and S1F). These data suggest that the BAC transgenic reporters we constructed faithfully marked the pluripotent state in ESC cultures and could be used to probe *Nanog* expression dynamics at single-cell resolution.

Next, we generated *Nanog:H2B-GFP* transgenic mice for single-cell resolution quantitative visualization of the EPI lineage in vivo. We used live imaging to analyze the distribution and validate the reporter in embryos (Figure 1C). We first observed reporter activity in embryos at the 8–16 cell stage (Plusa et al., 2008). Cells displaying high and low GFP levels were first observed at the mid blastocyst stage (70–100 cells), as a salt-and-pepper distribution of EPI and PrE precursors was established within the ICM (Chazaud et al., 2006; Plusa et al., 2008). In late blastocysts (>100 cells), where the EPI and PrE lineages have sorted into distinct layers, cells within the ICM forming the EPI exhibited significantly elevated levels of GFP compared to PrE cells located on the surface of the ICM. Thereafter, GFP was detected within the EPI, albeit at reduced levels in implanting E4.5 and post-implantation E5.5 embryos consistent with the downregulation of NANOG observed at periimplantation (Chambers et al., 2003). Notably, the reporter was strongly expressed in TE cells of early and mid blastocysts (corresponding to ~32–90 cell stage), possibly resulting from robust NANOG localization in ICM and TE cells at these stages (Figure S1I) (Dietrich and Hiiragi, 2007; Messerschmidt and Kemler, 2010; Morgani et al., 2013). However, GFP expression in the TE was significantly reduced in late (>100 cells) and in implanting blastocysts (Figures 1C and S1G). TE localization was also noted for other *Nanog*-based reporters analyzed at comparable embryonic stages (Figure S1G). Collectively, these data lead us to conclude that the *Nanog:H2B-GFP* reporter faithfully marks the pluripotent state both in vitro in ESC cultures and in vivo in the emerging EPI lineage of the mouse blastocyst.

### Derivation of ESCs from Mouse Blastocysts Results in Highly Variable Pluripotency-Associated Gene Expression

The EPI lineage of the blastocyst represents the in vivo counterpart to ESC cultures propagated in vitro (Boroviak et al., 2014). We therefore sought to investigate the profile of *Nanog:H2B-GFP* reporter activity in transgenic embryo-derived ESCs. We used an ESC derivation protocol in which an ICM outgrowth emerges in conditions promoting ground state pluripotency in serum-free medium containing 2i (Czechanski et al., 2014). Indeed, under these conditions GFP was strongly expressed by all cells of outgrowths from *Nanog:H2B-GFP*$^{Tg/+}$ blastocysts (Figure 1D). However, both reporter and NANOG expression became heterogeneous when the derived ESCs were propagated under standard serum+LIF conditions, either in the presence or absence of mouse embryonic feeders (MEFs). Even in the presence of MEFs, GFP-low/NANOG-low cells were observed within ESC colonies (Figure 1E). Fluorescence-activated cell sorting (FACS) and quantitative immunofluorescence analyses confirmed the presence of a highly heterogeneous

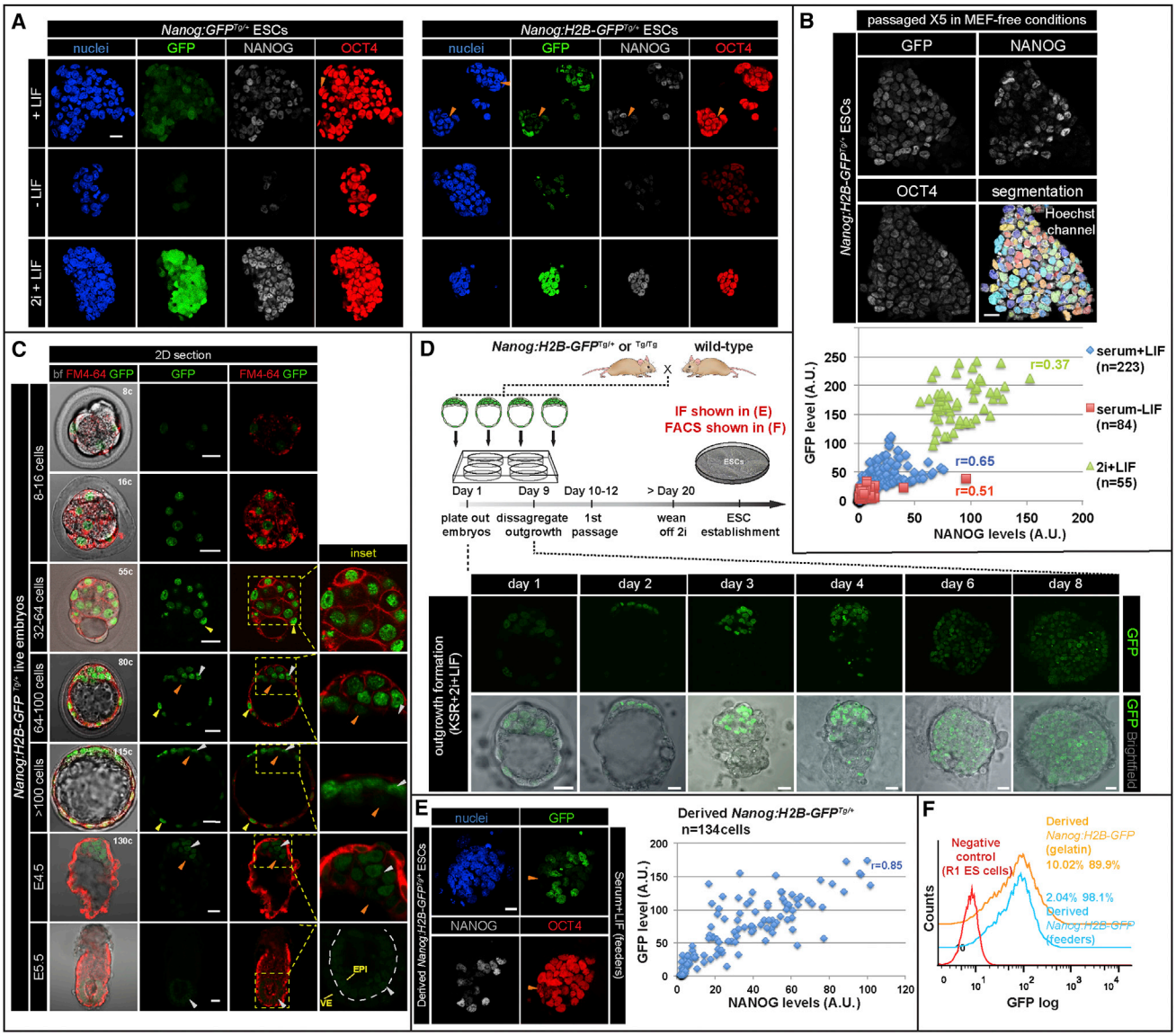


**Figure 1. BAC-Based *Nanog* Transcriptional Reporters Faithfully Mark the Pluripotent State in ESCs and Embryos**

(A) Immunofluorescence images of *Nanog:GFP*$^{Tg/+}$ and *Nanog:H2B-GFP*$^{Tg/+}$ ESCs grown in MEF-free conditions including serum+LIF, 2i+LIF, and serum-LIF for three passages. Orange arrowheads identify GFP-low and NANOG-low cells within ESC colonies.

(B) Quantitative immunofluorescence analysis after nuclear segmentation of *Nanog:H2B-GFP*$^{Tg/+}$ ESCs. GFP (y axis) and NANOG (x axis) fluorescence values plotted for individual ESCs propagated for five passages in MEF-free serum+LIF conditions then grown for 4 days in various culture conditions.

(C) Reporter expression in live embryos stained with membrane marker FM4-64. GFP-hi cells, white arrowheads; GFP-low cells, orange arrowheads; TE cells expressing GFP, yellow arrowheads. Dashed line depicts boundary between epiblast (EPI) and visceral endoderm (VE) layers of an E5.5 embryo. Cell number was determined by staining with Hoechst.

(D) Schematic of ESC derivation. After 20 days, *Nanog:H2B-GFP*$^{Tg/+}$ ESCs were established in the presence of MEF feeders in serum+LIF conditions and then propagated in the presence or absence of MEFs.

(E) Immunostaining and analysis of derived *Nanog:H2B-GFP*$^{Tg/+}$ ESCs. Orange arrowheads mark GFP-low/NANOG-low/OCT4$^{+}$ cells.

(F) FACS analysis of derived *Nanog:H2B-GFP*$^{Tg/+}$ ESCs grown in serum+LIF conditions in the presence or absence of MEFs. Numbers in FACS histograms indicate percentage of GFP$^{-}$ (left) and GFP$^{+}$ (right) populations. r = Pearson correlation coefficient. Scale bar represents 20 μm.

population, where both reporter and protein expression where highly correlated (r = 0.85) (Figures 1E and 1F). From these observations, we conclude that gene expression heterogeneities of the pluripotent state likely arise in ESCs as a result of their in vitro propagation.

## Quantitative Single-Cell Analysis of *Nanog:H2B-GFP* Expression in the Emerging Pluripotent Cells of the Blastocyst

To determine whether the transgenic reporter allowed a quantitative evaluation of *Nanog* expression in vivo, we analyzed the

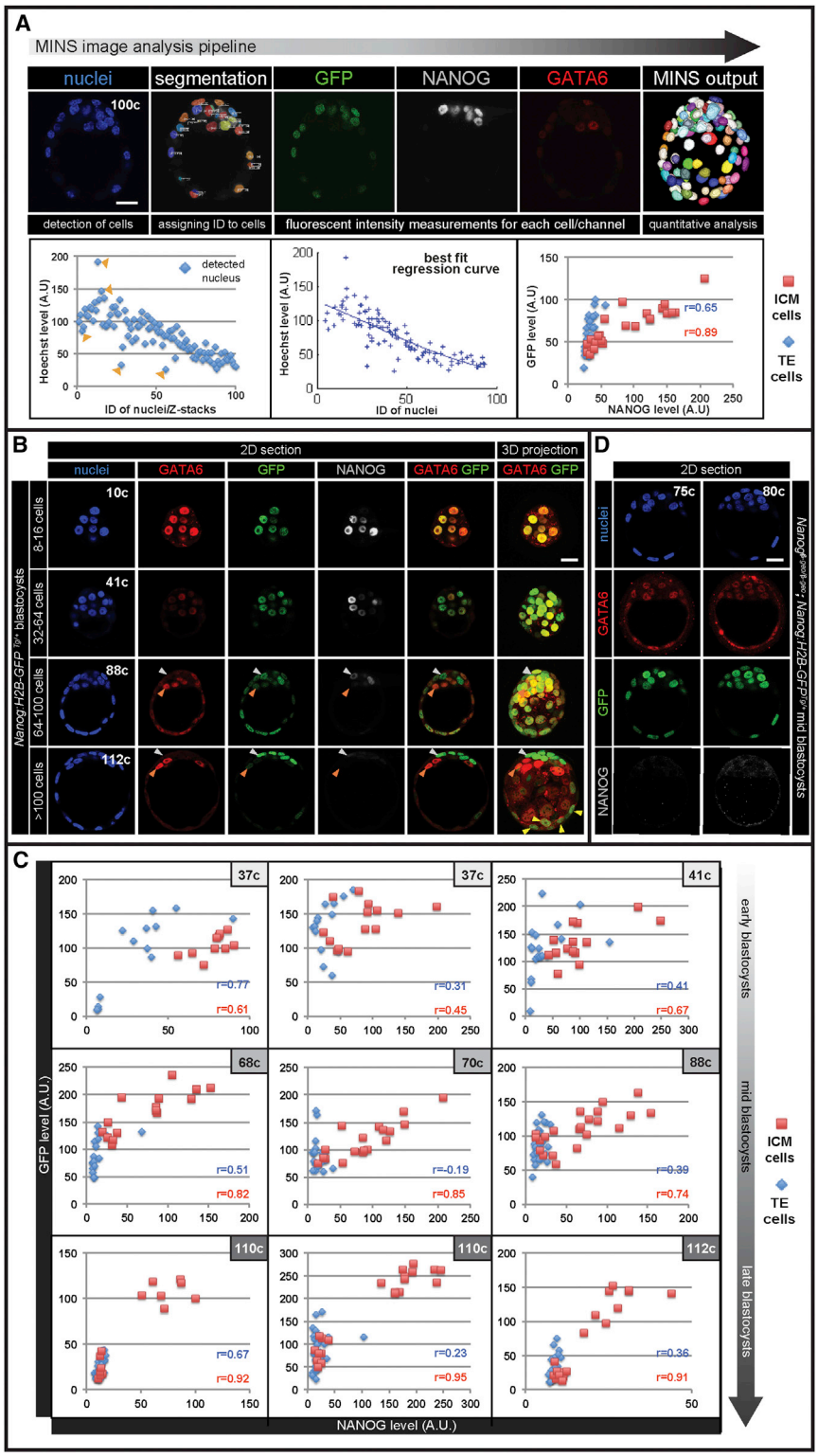


**Figure 2. Differential Expression of *Nanog:H2B-GFP* Reporter in Segregating EPI and PrE Cells**

(A) MINS image analysis pipeline (see Experimental Procedures). GFP and NANOG expression plotted for individual cells after automated nuclear segmentation and fluorescence intensity normalization (best-fit regression curve).

(B) Immunofluorescence images of fixed *Nanog:H2B-GFP*$^{Tg/+}$ embryos. EPI cells, white arrowheads; PrE cells, orange arrowheads; TE cells expressing GFP, yellow arrowheads.

(C) Quantitative immunofluorescence analyses.

(D) Reporter, GATA6, and NANOG expression in *Nanog*$^{\beta\text{-}geo/\beta\text{-}geo}$ blastocysts carrying the *Nanog:H2B-GFP* reporter. NANOG staining was absent in *Nanog* mutant transgenic embryos. r = Pearson correlation coefficient. Scale bar represents 20 μm.

pattern of reporter expression in transgenic embryos that had been fixed and stained for lineage-specific markers such as GATA6/PrE and NANOG/EPI using single-cell quantitative image analysis (Lou et al., 2014) (Figure 2A). In morulae (8-16 cells) and early blastocyst (32–64 cells) stages, GFP was observed throughout the embryo, reflecting a double (GATA6$^+$ NANOG$^+$) -positive state. The differential levels of GFP expression were evident in mid blastocysts (~70–100 cells), as embryos established a mutually exclusive distribution of GATA6$^+$ PrE and NANOG$^+$ EPI progenitors (Figures 2B and S2A). In late blastocysts (>100 cells), where the EPI/PrE sorting had occurred, reporter expression was markedly elevated in NANOG$^+$ EPI progenitor cells and diminished in GATA6$^+$ PrE progenitor cells (Figure 2B). Quantitative fluorescence analysis of immunostained *Nanog:H2B-GFP*$^{Tg/+}$ blastocysts at different stages confirmed a strong correlation between GFP and NANOG levels in ICM cells, as seen in ESCs, thus indicating that the reporter could be used to quantitatively infer levels of expression of *Nanog* (Figures 2C and S2B). Notably, reporter expression in TE cells was prominent in early and mid blastocysts but displayed reduced correlation with NANOG protein compared to the ICM and hence was not investigated further (Figures 2C and S2B). The H2B-GFP reporter responds to changes in *Nanog* expression with a characteristic time that is determined by the stability of the H2B-GFP fusion protein. Our control experiments and computational analysis indicate that we can measure changes in *Nanog* expression higher than 2-fold with about 1 hr resolution (see the Supplemental Experimental Procedures). Such temporal resolution is

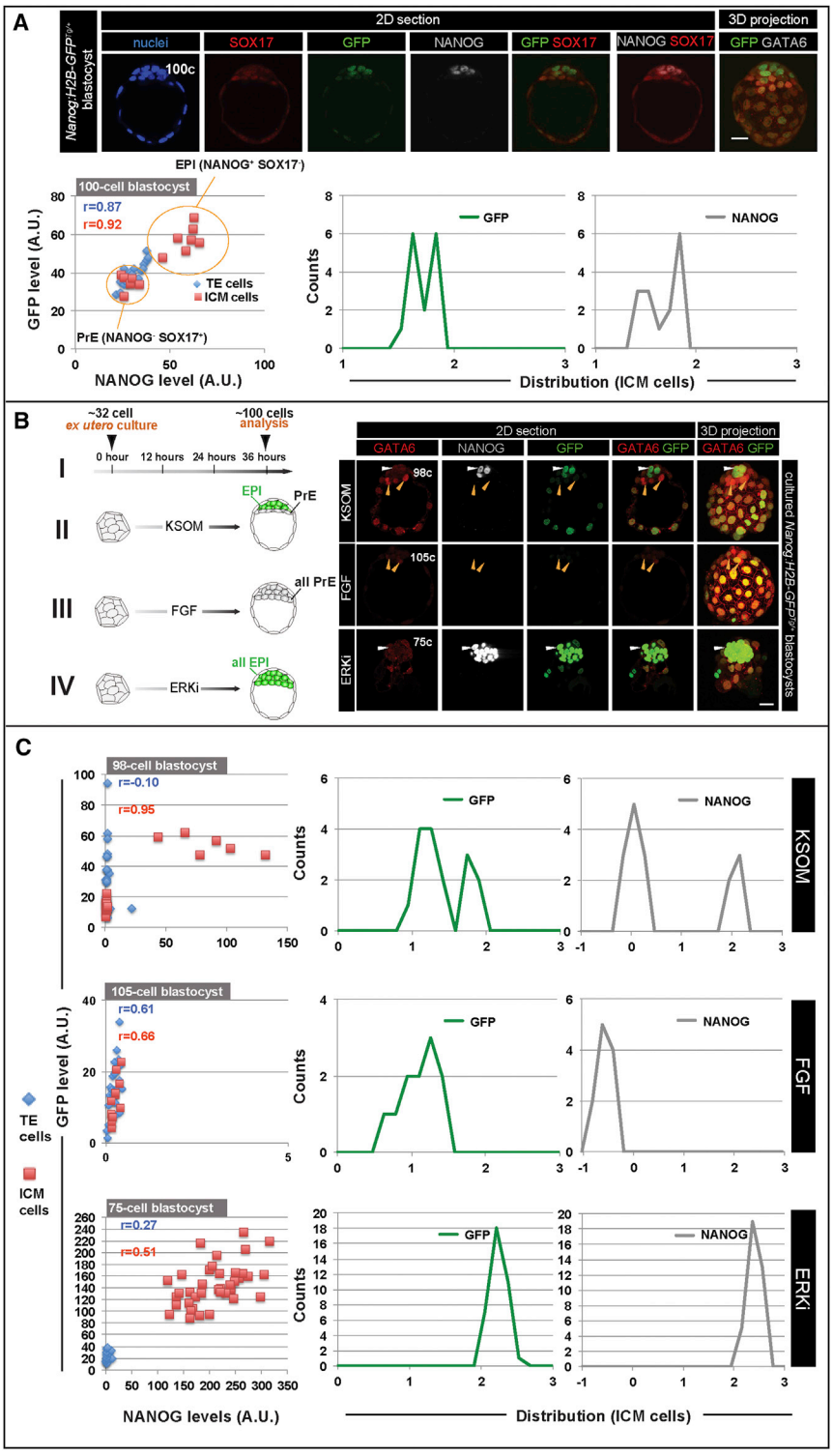


**Figure 3. *Nanog* Expression in the ICM Is Altered by Modulation of FGF Signaling**

(A) Immunofluorescence images of late blastocyst stage *Nanog:H2B-GFP*$^{Tg/+}$ embryo. Fluorescence values for GFP and NANOG plotted for individual cells. Values for GFP and NANOG of ICM cells also plotted as frequency distributions obtained by binning fluorescence values in 20 logarithmically spaced categories, as described previously (Muñoz Descalzo et al., 2012).

(B) Regimen used for exogenous FGF and ERK1/2 inhibitor (ERKi) treatment experiments. *Nanog:H2B-GFP*$^{Tg/+}$ blastocysts recovered at E2.75 and cultured for 36 hr in KSOM medium (I), KSOM + FGF2 (II), and ERKi (III), followed by staining for Hoechst, NANOG, and SOX17. White arrowheads identify NANOG$^{+}$;SOX17$^{-}$ ICM cells exhibiting high levels of GFP. Orange arrowheads identify SOX17$^{+}$;NANOG$^{-}$;GFP-low ICM cells.

(C) Reporter and NANOG distribution analysis in cells of cultured embryos shown in (B).

Note that x and y axis scales for scatterplots vary due to changes in reporter and NANOG expression between embryos cultured under different conditions. r = Pearson correlation coefficient. Scale bar represents 20 μm.

much smaller than the timescales of cell differentiation. Finally, by analyzing *Nanog* mutant embryos carrying the reporter, we confirmed that no functional NANOG protein was produced from the BAC transgene (Figure 2D). We therefore conclude that the *Nanog:H2B-GFP* reporter faithfully marks pluripotent cells emerging within the ICM and provides an accurate quantitative readout of *Nanog* expression.

## Distribution of NANOG Expression in the Blastocyst Is Altered by Modulation of Fibroblast Growth Factor Signaling

Next, we investigated the distribution of the *Nanog:H2B-GFP* transcriptional reporter, as well as NANOG protein, as the EPI compartment emerges within the ICM of late blastocysts. We performed quantitative immunofluorescence analysis on mid-to-late blastocysts (90–110 cells), stained with Hoechst, NANOG, and the PrE marker SOX17 (Figure 3A). We noted a bimodal distribution of reporter expression within the ICM, which corresponded to bimodality in NANOG distribution within prospective EPI and PrE cells (Figures 3A and S3A–S3D).

We investigated how these distributions could be modulated by perturbation of fibroblast growth factor (FGF) signaling, which plays a critical role in ICM lineage choice. Pathway inhibition results in an ICM composed exclusively of EPI precursors, while incubation of embryos in exogenous FGF results in an all-PrE ICM (Chazaud et al., 2006; Kang et al., 2013; Nichols et al., 2009; Yamanaka et al., 2010). Consistent with these studies, we observed that the bimodal distribution of GFP and NANOG levels within the

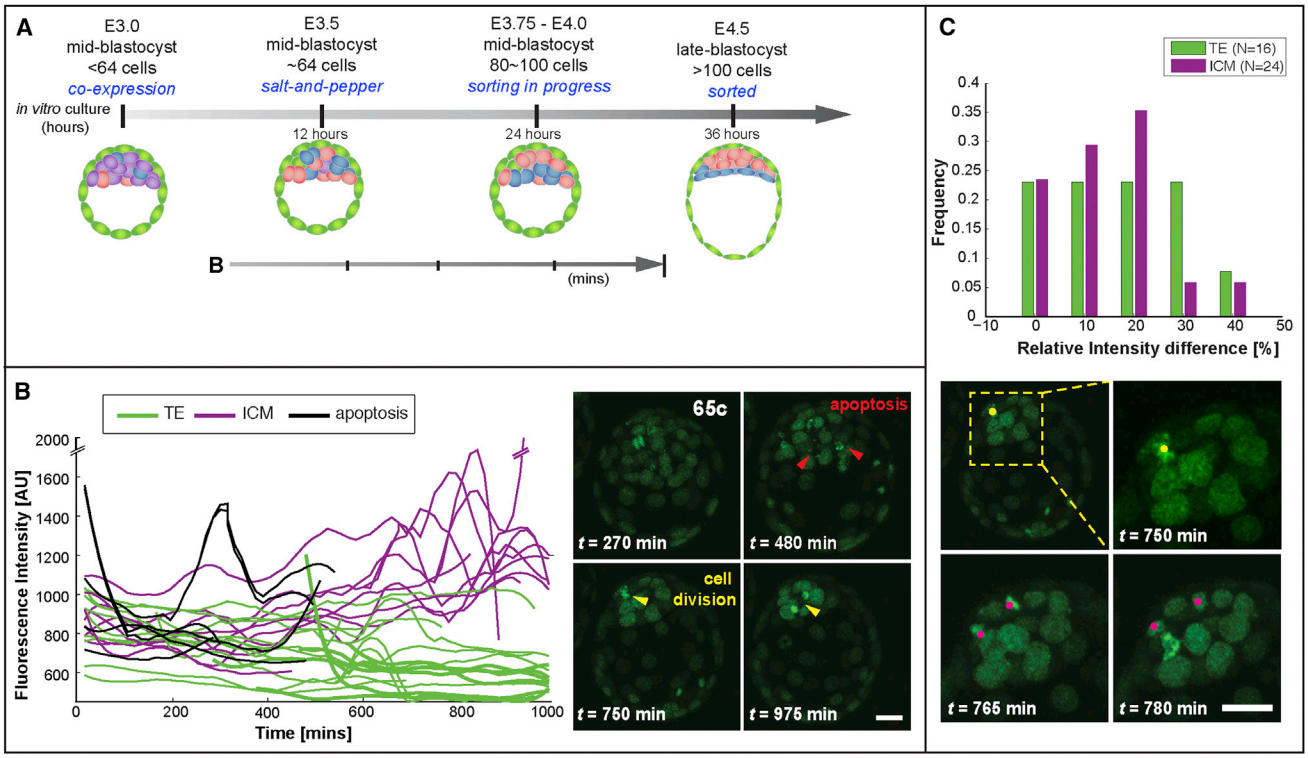


**Figure 4. EPI Cells Emerge In Vivo with an Accompanying Increase in *Nanog* Expression**

(A) Schematic of mouse blastocyst stage embryo development.

(B) Quantification of GFP intensity in individual nuclei of a living *Nanog:H2B-GFP*$^{Tg/+}$ blastocyst recovered at E3.5 (65 cells) and corresponding images of single time points. Single-cell intensity traces were obtained by tracking single cells in time-lapse experiments. Mitotic and apoptotic cells were also tracked, resulting in abrupt peaks in fluorescence intensity. Cells belonging to the ICM are depicted in purple, while TE cells are depicted in green; cells having undergone apoptosis are depicted as black lines. The developmental timing and the time spanned by tracks analyzed in this panel are illustrated by an arrow in (A).

(C) Top panel, quantification of relative GFP intensity in daughters/sisters versus mother cells upon division in cells of TE (green bars) or ICM (purple bars) origin. Daughter cells retained expression levels after mitosis, with most changes within 20%.

Data were obtained from the analysis of time-lapse movies of five or more embryos. Bottom panel, cell divisions of EPI progenitors occurring at late blastocyst stages shown in (B). Red arrowheads identify apoptotic events, and yellow arrowheads mark cell divisions. Scale bar represents 20 μm.

ICM was lost when FGF signaling activity was modulated (Figures 3B, 3C, and S3E–S3J). We therefore conclude that a heterogeneous distribution of NANOG expression exists in vivo. This is represented as a stable bimodal distribution within the ICM and reflects cell fate specification toward PrE and EPI lineages, and that this distribution is altered by modulation of FGF signaling.

## Highly Variable *Nanog* Dynamics Are Initially Observed Followed by the Establishment of Differential Expression at the Onset of ICM Lineage Specification

A bimodal distribution of *Nanog* expression is established as the pluripotent EPI emerges within the ICM. However, we currently do not know whether fluctuating expression of pluripotency-associated factors, such as *Nanog*, occurs during EPI specification, nor, if they do exist, whether such fluctuations correlate or predict state reversions (Smith, 2013). To address this question, we investigated the behavior of individual ICM cells in *Nanog:H2B-GFP*$^{Tg/+}$ blastocysts using time-lapse imaging coupled with quantitative image analyses performed in an accurate and automated fashion (Supplemental Experimental Procedures).

Using this methodology, we first observed that in early blastocysts (until ~60 cell stage) all cells (ICM and TE) displayed highly heterogeneous reporter activity (0–400 min in Figure 4B), consistent with previous observations (Dietrich and Hiiragi, 2007; Ohnishi et al., 2014; Plusa et al., 2008). Following this phase, TE cells downregulated reporter expression, whereas ICM cells retained or increased their expression, presumably coinciding with the establishment of a lineage bias (400 min to end of movie; Figure 4B). We also noted apoptotic events, occurring during the process of lineage specification in randomly positioned GFP-hi or GFP-low ICM cells (red arrowheads; Figure 4B). As described previously, apoptotic events occur during blastocyst development and are not a consequence of in vitro culture or phototoxicity (Artus et al., 2013; Plusa et al., 2008). Furthermore, we noted several cell divisions occurring in GFP-hi ICM cells (yellow arrowheads; Figure 4B). Heritability of *Nanog:H2B-GFP* levels, and likely cell fate, was observed in all ICM cells after division (Figure 4C). Of note, an increase in GFP fluorescence was routinely observed during mitosis, due to chromosome condensation; thus any resulting rapid oscillations (of the order of 150 min) in reporter activity were excluded from the analysis, as they were not

considered as reflecting changes in gene expression. By using a computational approach, we confirmed that GFP expression was not diluted in dividing cells, suggesting that daughter cells inherited the lineage identity of their parental cell (Figure S4). Finally, cells within the TE displayed low, somewhat variable and continually decreasing levels of reporter activity (Figure 4B).

Next, we focused our analyses on subsequent phases of development, initiating from early-to-mid blastocyst stages (at around 50–60 cell) until late blastocyst stages (at around 100 cells), where the EPI and PrE cells have sorted to their final positions (Figures 5A and 5B; Movie S1). A subpopulation of ICM cells is specified to the EPI-lineage, with GFP expression maintained or increased. By contrast, cells biased toward the PrE lineage extinguished the reporter during differentiation (Figure 5A).

## Infrequent Cell-State Reversals Occur toward, Not Away from, a Pluripotent Identity

Notably, we observed a few instances where cells in mid-stage blastocysts, exhibiting low levels of reporter activity, would rapidly increase reporter activity, and concomitantly become segregated with the EPI (Figure 5A). These could, in principle, represent rare PrE-to-EPI conversions. Importantly, we never observed events of EPI-to-PrE progenitor switching associated with downregulation of *Nanog* expression. To obtain an independent confirmation of the absence of EPI-to-PrE transitions, we analyzed time-lapse data from a PrE-specific single-cell resolution reporter (*Pdgfra*$^{H2B\text{-}GFP/+}$, Plusa et al., 2008). In contrast to *Nanog:H2B-GFP*, expression of the *Pdgfra*$^{H2B\text{-}GFP}$ reporter is activated only in PrE-biased cells after cell-fate specification. Therefore, PrE-to-EPI conversion would be detected as downregulation of the reporter. On the other hand, EPI-to-PrE conversion would give rise to significantly delayed activation of the reporter in cells lacking expression. We imaged embryos expressing the *Pdgfra*$^{H2B\text{-}GFP}$ reporter starting at the time of cell differentiation, i.e., the time when expression of the reporter becomes reliably detectable. We found that all positive cells at the onset of differentiation retained their expression and no new cells initiated expression with a significant delay, corresponding to an EPI-to-PrE conversion (Figure 5B). Collectively, our results with the *Nanog:H2B-GFP* and *Pdgfra*$^{H2B\text{-}GFP/+}$ reporters imply that cell-fate reversals are extremely rare and preferentially happen from the PrE to the EPI state.

The PrE-to-EPI unidirectionality would suggest that fate transitions are regulated and do not result from purely stochastic fluctuations in gene expression. To rule out that the inability to detect EPI-to-PrE transition in *Nanog:H2B-GFP* embryos was due to perdurance of GFP reporter, we performed the following analysis. First, we quantified the dynamics of downregulation of *Nanog:H2B-GFP* in PrE cells (Figure S6) and estimated the lifetime of H2B-GFP to be shorter than 4 hr, which is short enough to detect cell-fate reversal events (details in the Supplemental Experimental Procedures). Second, we analyzed time-lapse movies of the *Nanog:H2B-GFP* reporter in embryos treated with exogenous FGF (all ICM cells would downregulate NANOG) and showed that a clear downregulation can be observed (Figure S5). In addition, we calculated the half-life of H2B-GFP from time-lapse movies of *Nanog:H2B-GFP* in exogenous FGF or cycloheximide (CHX). The decay rates of H2B-GFP in ICM cells in the embryos under CHX or FGF treatments were around 6.5 and 5.5 hr, respectively (Figure S6). Collectively, these experiments allow us to conclude that the half-life of H2B-GFP is shorter than 6 hr and thus not dissimilar to the half-life of NANOG, which has been calculated to be approximately 4 hr (Abranches et al., 2013). Altogether, these results show that the *Nanog:H2B-GFP* reporter allows measuring *Nanog* transcriptional dynamics on timescales longer than 1 hr (see the Supplemental Experimental Procedures).

## At Late Blastocyst Stages, EPI and PrE Do Not Exhibit Fluctuations

Next, we examined whether fluctuations in *Nanog:H2B-GFP*, and thus *Nanog*, levels were observed after ICM lineage specification. At these late blastocyst stages (>90–100 cells), the active sorting of EPI and PrE populations to adjacent tissue layers is evident. Our analyses revealed that the EPI cells exhibited increasing levels of reporter activity, whereas a decrease in GFP levels was observed in cells forming the emergent PrE epithelial layer (0 min to end of movie; Figure 5C; Movie S1). At the end of the specification period, apoptotic events were observed (red arrowhead; 0–100 min; Figure 5C). Thereafter, we did not observe any apoptosis. Instead, after ICM lineage specification, several cell divisions were observed in EPI progenitors (yellow arrowheads; Figure 5C). Collectively, these observations suggest a wave of temporarily restricted apoptotic events, occurring around the period of lineage specification, followed by a burst of EPI lineage-specific cell proliferation. *Nanog* levels remained stable after ICM cell-fate divergence suggesting that fluctuations between EPI and PrE states do not occur. Based on these data, we conclude that within the ICM the majority of pluripotent EPI and extra-embryonic PrE progenitor cells do not change their fate after specification. Furthermore, our data lead us to propose that a burst of cell proliferation following cell differentiation ensures EPI lineage-specific expansion.

## Quantitative Analyses of *Nanog:H2B-GFP* Time-Lapse Movies Revealed a Correlation between Cell Behaviors and Cell-Fate Choice within the ICM

Time-lapse imaging in combination with cell tracking and quantitative analysis allowed us to determine whether fate reversals correlate with the spatial position of individual cells within the ICM. We simultaneously analyzed the position of a cell relative to the blastocyst cavity, and its *Nanog* reporter expression levels as a function of time. Analysis of the spatial distribution of cells converting from PrE-to-EPI indicated that the cells migrated toward the inner region of the ICM (Figure 6A, blue cell). The cell undergoing fate switching exhibited similar rate of GFP increase as in cells of the embryo under conditions of ERK inhibition (Figure 6B). This observation suggests that the fate switching might be a result of PrE-biased cells that stop responding to ERK signaling (due to their localization and fates of their neighbors) and, as a consequence, increase *Nanog* expression and change fate. Consistently, under conditions of ERK inhibition, all ICM cells committed to an EPI fate and displayed increasing reporter activity, whereas GFP expression in TE cells remained unaffected, consistent with our previous observations in fixed embryos (Figures 3B, 3C, and S3E–S3J). Notably, we did not

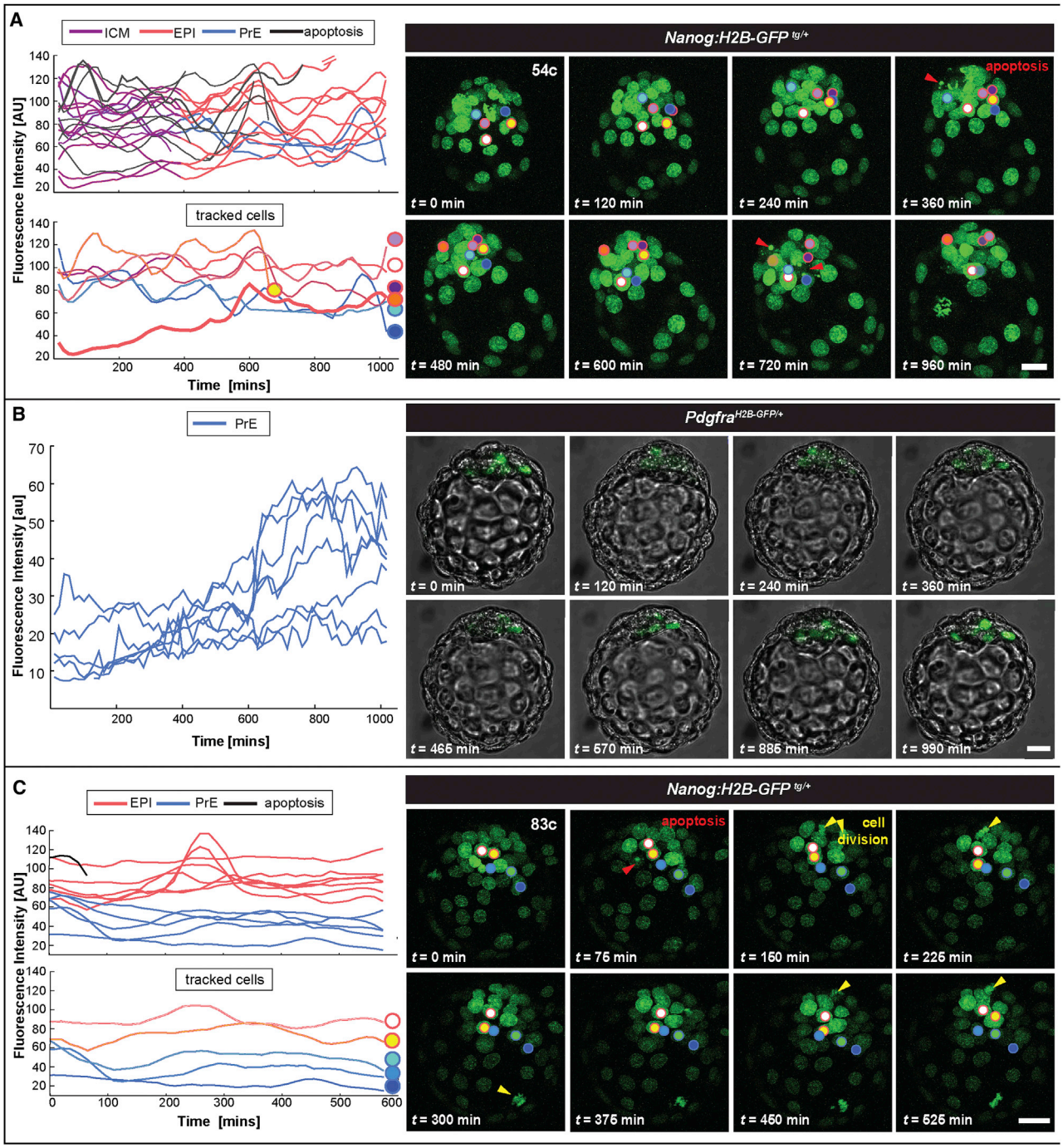


**Figure 5. State Reversals Can Occur toward a Pluripotent Identity during Lineage Specification in Mid Blastocysts, but Cells Do Not Change Fate in Late Embryos**

(A) Quantification of GFP intensity in single nuclei of a living *Nanog:H2B-GFP*$^{Tg/+}$ at E3.5 (54 cells) and corresponding snapshots from a time-lapse movie. A subset of tracks are detailed in the lower plot, corresponding to cells highlighted in the images in the panel on the right. Cell highlighted with an orange dot and red outline represents a GFP-low cell that upregulated reporter expression and contributed to EPI.

(B) Quantification of GFP intensity in single nuclei of a living *Pdgfra*$^{H2B\text{-}GFP/+}$ at E3.5 (~60 cells) and corresponding snapshot of fluorescence channel overlapped with bright-field images from a time-lapse movie. Only PrE-biased cells express H2B-GFP.

(C) The same analysis applied in (A) was repeated in a later *Nanog:H2B-GFP*$^{Tg/+}$ embryo at E3.75 (85 cells). ICM cells segregated toward EPI (red) and PrE (blue) lineages. Cells that underwent apoptosis depicted with black lines. Red arrowheads mark apoptotic events and yellow arrowheads mark cell divisions. Tracked nuclei are highlighted by dots; the outline of each dot depicts the lineage choice; red outline depicts EPI progenitor cells; blue outline depicts PrE progenitor cells. Scale bar represents 20 μm.

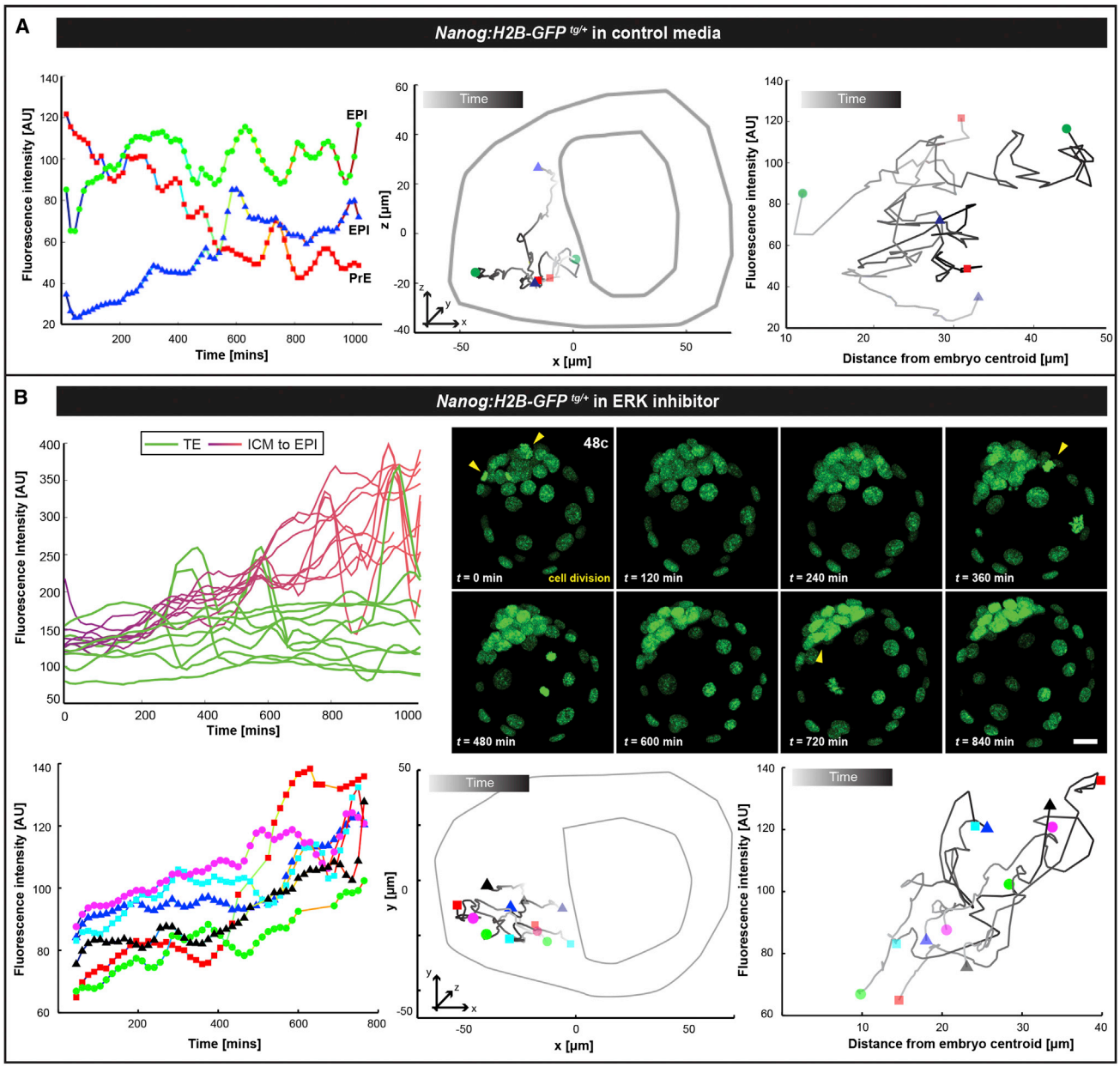


**Figure 6. Cell-State Reversals toward a Pluripotent Identity Are Associated with Changes in Position within ICM**

Fluorescence levels of single ICM cells (A, left, and B, lower-left panels) and two-dimensional projections of representative space trajectories (A, central, and B, lower-central panels) are plotted for the duration of time-lapse movies of *Nanog:H2B-GFP*$^{Tg/+}$ embryo (A) corresponding to embryo in Figure 5A and (B) in the presence of ERKi. The distance of each cell from the barycenter of the embryo is plotted versus GFP intensity (A, right, and B, lower right).

(A) EPI cells, green and blue; PrE cell, red trajectories. Blue trajectory represents a cell that switched state acquiring an EPI identity, moving from an initial position on the surface of ICM inward while increasing *Nanog* expression.

(B) Top, quantification of GFP fluorescence intensities and corresponding snapshots. Bottom, all six trajectories depict the behavior of ICM cells that acquire an EPI fate increasing reporter activity. All cells change their absolute position due to embryo growth, but there are no events of abrupt spatial change in position of individual cells within the cohort. Lines represent cell trajectories. Displayed trajectories for mitotic cells were excluded. Unique colors identify individual cells. The outline of the embryo is drawn for plotting relative position of nuclei. Shades of gray in the trajectory depict time: earlier (light) to later (darker).

observe any apoptotic events during ERK inhibition, whereas a burst of proliferation was evident in the all-EPI ICM (yellow arrowheads in Figure 6B and Movie S2). These findings support our previous observations, suggesting that apoptosis serves as a selection mechanism within the ICM, while the proliferation burst in EPI-committed cells ensures the rapid expansion of

the pluripotent lineage after its specification. In addition, we observed that there was no abrupt spatial position change of EPI cells within the ICM of ERK inhibitor-treated embryos; instead, cell motility was restrained, and only passive cell movement was observed as these embryos developed (Figure 6B).

## DISCUSSION

Pluripotency-associated factors such as *Nanog* have been reported to exhibit dynamic fluctuations of expression in ESC cultures. Whether fluctuations in gene expression correlating with cell-state transitions occur in vivo remains an open question. Here, we have investigated *Nanog* expression heterogeneities using single-cell resolution *Nanog* transcriptional reporters coupled with 3D time-lapse imaging and high-resolution automated quantitative image analyses. Our data suggest that BAC-based *Nanog:H2B-GFP* transgenic reporters are expressed at physiological levels, exhibit minimal reporter perdurance, and serve as a faithful readout of *Nanog* expression both in vitro in ESCs, and in vivo in mouse embryos.

For both ESCs rendered transgenic through introduction of a *Nanog:H2B-GFP* construct, as well as transgenic embryo-derived ESCs, heterogeneities in the levels of reporter, as well as NANOG protein, were noted. A GFP-low cell population, which also displayed low levels of NANOG protein, was evident in cells that were propagated in MEF-free conditions, which promote a differentiation bias; this population displayed OCT4 expression (Figure 1A, 1B, and S1E), suggesting that it might consist of pluripotent cells that were actively differentiating and/or primed for differentiation. Importantly, this variability, and the presence of a GFP-low/NANOG-low population, in ESC cultures have also been recently reported with another *Nanog* transcriptional reporter (Abranches et al., 2013). These observations therefore call for caution in the choice of culture conditions for ESC propagation; hence, it was recently shown that random monoallelic gene expression could occur stochastically as ESCs differentiated, resulting in the acquisition of heterogeneities during the adaptation of cells to in vitro culture (Eckersley-Maslin et al., 2014; Gendrel et al., 2014).

Furthermore, it has been suggested that reporters targeted to the *Nanog* locus, which concomitantly ablate *Nanog* activity, might exhibit behaviors resulting from *Nanog* heterozygosity (Faddah et al., 2013; Filipczyk et al., 2013). We noted that GFP expression from the knockin/knockout TNGA reporter was elevated compared to a BAC-based *Nanog:GFP*$^{Tg/+}$ reporter (Figures S1A–S1C). We therefore investigated whether *Nanog* allele heterozygosity per se might result in increased NANOG expression, consistent with its reported auto-repressive activity (MacArthur et al., 2012; Navarro et al., 2012). However, we failed to observe any noticeable difference in reporter activity between *Nanog:H2B-GFP*$^{Tg/+}$ ESCs that harbored a two (wild-type) or one functional *Nanog* alleles (Figures S1J and S1K). Thus, our data suggest that the elevated GFP expression observed in the TNGA ESCs is not the result of *Nanog* heterozygosity, and could result from allele design. The development of a faithful EPI lineage-specific reporter providing a single-cell resolution quantitative readout of *Nanog* expression, coupled with high-resolution image data analyses allowed us to address a central open question pertaining the behavior of EPI cells in vivo. Critical for this type of analysis was a single-cell resolution live imaging reporter that was sufficiently bright for time-lapse image acquisition, but expressed at physiological levels, so that reporter perdurance would not mask downregulation in cells. Notably, our experience with destabilized fluorescent protein reporters reveals reduced levels of fluorescence, not amenable to the image analyses methodologies used in this study.

Our data reveal a range of cell behaviors before and after the pluripotent EPI population has been specified in vivo within the ICM (Figure 7). Prior to EPI versus PrE specification has occurred, apoptosis serves as a selective mechanism to ensure proper segregation of lineage progenitors. Rare fate reversal events likely occur whereby GFP-low/PrE progenitor cells convert to a GFP-hi/EPI progenitor state as cells migrate inward in the ICM. At this time, cell migration correlates with fate choice and is linked to the presence of a heterogeneous population of EPI and PrE progenitors. Progenitors could be sorting toward a niche comprising cells with a similar lineage bias. By contrast, in the presence of ERK inhibition, lineage choice is forced toward one direction (all-EPI) resulting in a homogenous ICM population and is accompanied by a lack of cell movement (Figure 6B). Finally, after lineage specification has occurred within the ICM, fluctuations between EPI and PrE progenitors were not observed. However, a burst of cell proliferation was observed in EPI progenitors, as they sorted to the interior of the ICM.

Rarely cells changed their state toward, but never away from, a pluripotent identity. By using a single-cell resolution reporter for the PrE lineage, we previously showed that PrE progenitor cells could downregulate reporter expression but could not confirm the fate reversal to EPI, as cells could not be followed after loss of the reporter (Plusa et al., 2008). Here, by using a single-cell resolution reporter of the EPI lineage, we directly visualized these transitions. Perhaps cells converting from PrE-to-EPI might cease responding to an FGF signal, as in the presence of an ERK-inhibitor, resulting in *Nanog* upregulation and establishment of pluripotency. These data agree with recent studies suggesting that pulsatile FGF signaling induces differential *Nanog* expression within ICM cells and drives *Nanog* mRNA degradation for rapid post-transcriptional control of pluripotency (Torres-Padilla and Chambers, 2014; Tan and Elowitz, 2014).

Importantly, we observed no fate reversals between EPI and PrE subsequent to their specification. This is in agreement with a recent mathematical model accounting for the dynamics of the regulatory network that controls ICM differentiation; simulations indicated that after specification cells would not change identity, and thus EPI and PrE states are not interchangeable (Bessonnard et al., 2014). In addition, we observed that after specification a burst of cell proliferation in the pluripotent compartment was evident. This might ensure adequate numbers of EPI progenitors available for subsequent development. Furthermore, our observations suggest that PrE progenitors exhibit increased plasticity, compared to EPI progenitors, consistent with recent studies suggesting that PrE progenitors have a broader developmental potential than their EPI counterparts (Grabarek et al., 2012), and observations reporting that

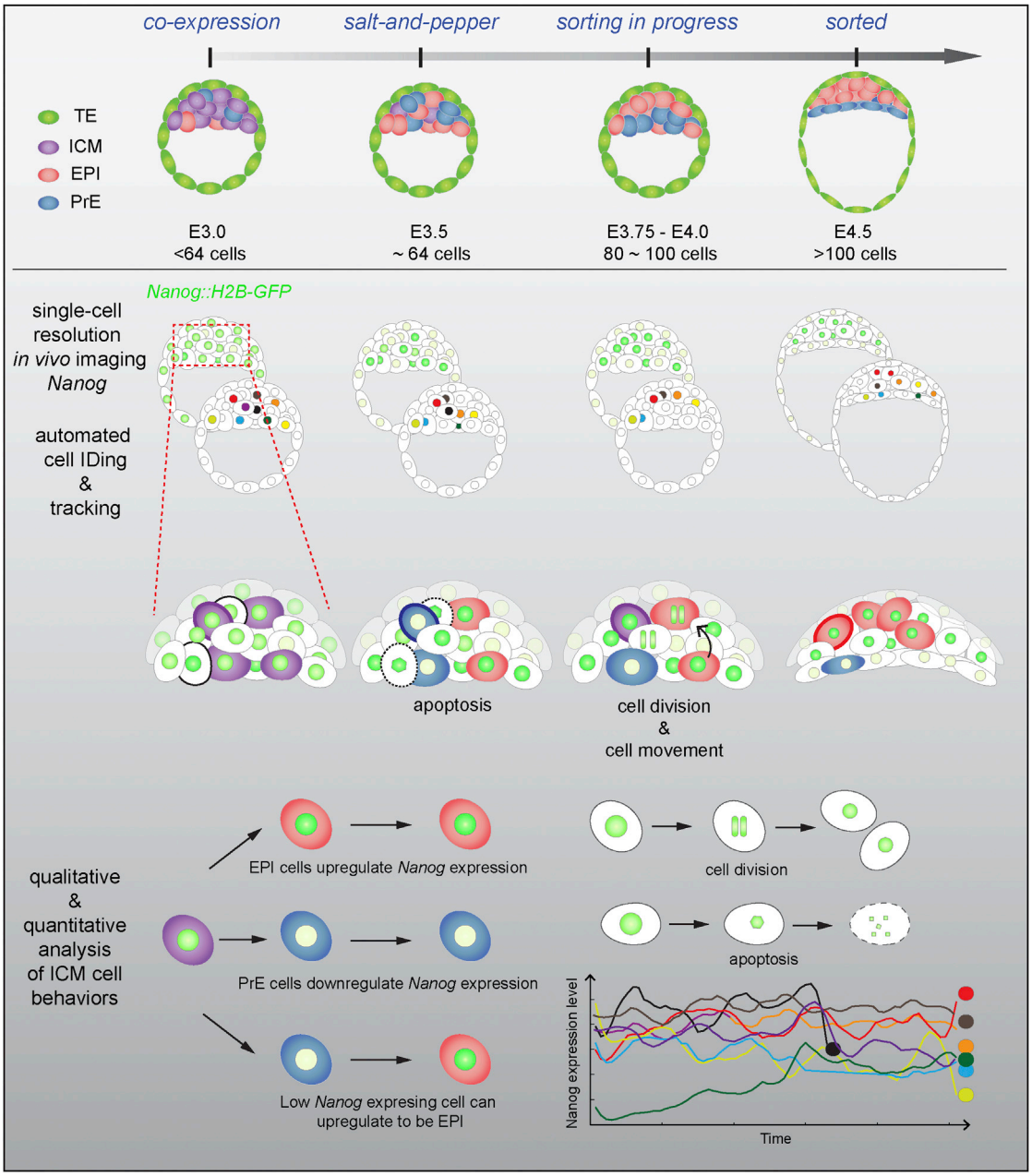


**Figure 7. Cell Behaviors during the Emergence of the Pluripotent EPI Lineage**

Schematic representation of embryo development from mid-to-late blastocyst. Prior to lineage specification (around 64–80 cells): (1) apoptosis occurs randomly in EPI or PrE progenitors as they segregate to their appropriate layers, (2) segregation is linked to spatial movements within the ICM, and (3) few GFP-low cells might acquire a pluripotent identity and migrate inward the ICM. After lineage specification (>80–90 cells): (1) cells do not fluctuate between EPI and PrE states, and (2) cell divisions occur in EPI-specified population while relocating to the interior of the ICM.

ESCs are primed toward endoderm co-express embryonic and extra-embryonic markers (Morgani et al., 2013).

Our data suggest that once specified in wild-type embryos, pluripotent cells do not, in general, change their fate. However, a very limited number of state reversals may occur at this time, but only toward a pluripotent identity. During development, sufficient numbers of lineage progenitors must be generated, and there is a time window during which cell-fate reversals can occur. Moreover, mechanisms involving apoptotic events and symmetric cell divisions may ensure that a pluripotent identity is protected and maintained in vivo. These observations within the embryonic environment appear contrasting with studies in ESCs. A possible explanation for this apparent disparity could be that ESCs in culture do not receive the appropriate inputs

from a niche, namely, neighboring cells and extra-cellular components. Another could be due to the differential timescales. ICM cells commit to PrE and EPI fates in less than 24 hr, and, since development proceeds unidirectionally, even though there may be non-differentiating (or symmetric) cell divisions, neither cell population arising within the ICM self-renews. By contrast, ESCs can be maintained indefinitely in vitro under conditions of self-renewal, a timescale that presents an unrestricted period for conversion between alternative states.

## EXPERIMENTAL PROCEDURES

### Mouse Husbandry

All animal experiments were approved by the Institutional Animal Care and Use Committee at the Memorial Sloan Kettering Cancer Center. Mice were maintained under a 12-hr light-dark cycle. Mouse lines used in this study were *Nanog:H2B-GFP*$^{Tg/+}$, *Nanog*$^{\beta\text{-}geo/+}$ (Mitsui et al., 2003), and *Nanog*$^{GFP/+}$ (Hatano et al., 2005). Alleles are schematized in Figure S1H.

### Live Embryo Imaging

For live imaging, embryos were cultured in glass-bottomed dishes (MatTek) in an environmental chamber as done previously (Kang et al., 2013). Live imaging conditions used were compatible with normal development as shown previously (Plusa et al., 2008). For incubation experiments, an ERK1/ERK2 inhibitor, 1 μM PD0325901 (StemGent), was added to medium 2–3 hr prior to initiation of 3D time-lapse imaging. GFP was excited using a 488-nm Argon laser. Live image data were acquired using four laser scanning confocal imaging systems: Zeiss LSM510META, LSM710, LSM780, and Leica SP8. Images were acquired using 20×/0.75, 40×/1.3, or 63×/1.4 objectives. 20–30 xy planes separated by 2 μm were acquired per z stack, every 15 min. Movies of 3D time-lapse sequences were compiled and annotated using QuickTime Pro (Apple).

### Immunostaining of ESCs and Embryos

Immunostaining of ESCs and embryos was performed as previously (Kalmar et al., 2009; Kang et al., 2013; Muñoz Descalzo et al., 2012). Primary antibodies used were CDX2 (1:100, Biogenex), GATA6 (1:100, R&D Systems), NANOG (1:500, Cosmo Bio), OCT4 (1:100, Santa Cruz Biotechnology), and SOX17 (1:100, R&D Systems). Secondary Alexa Fluor (Invitrogen) conjugated antibodies were used at 1:500. DNA was visualized with Hoechst 33342 (5 μg/ml; Invitrogen).

### Quantitative Fluorescence Image Analysis

Quantitative fluorescence measurements from images of fixed ESCs and fixed or live embryos were performed using an automated image processing workflow comprising the segmentation of multiple nuclei in 3D data (Figure 2A). The front-end software, MINS, is a MATLAB (MathWorks)-based graphic user interface described previously (Lou et al., 2014; http://katlab-tools.org). We noted that for normalizing fluorescence values of each channel the Hoechst channel per cell was not optimal to compensate for loss of fluorescence intensity throughout the sample depth (differences in Hoechst fluorescence intensity throughout z stack indicated by orange arrowheads in Figure 2A). We thus developed an algorithm to generate a regression curve across values of the Hoechst channel for individual cells (details in the Supplemental Experimental Procedures). Fluorescence values for other channels were normalized using this curve (Figure 2A). To compare fluorescence values between ICM and TE cells, TE cells being analyzed needed to be in the same focal plane as ICM cells. Thus, TE cells positioned at the beginning and end of the z stack were excluded from the analysis. Only accurately segmented nuclei were included in analyses.

### Nuclear Segmentation and Cell Tracking

Using the segmentation output of the MINS software, we developed an algorithm for cell tracking. To determine the position of any given cell at a subsequent time point, the algorithm first seeks to identify a clear, well-defined minimum in the distance between the cell centroid and the centroids of all cells in the subsequent frame. If such minimum does not exist, the algorithm uses cell segmentation to look for maximum overlap between cells at the subsequent time point and the cell being tracked. As additional criteria, changes in nuclear shape and overall distance are required to lie within control ranges. Such criteria generate unambiguous cell assignments and provide reliable tracking of a large fraction of cells (60%–70% in this study). The algorithm was validated by visual inspection, and each track was obtained by matching forward (prospective) and reverse (retrospective) tracking data (details provided in the Supplemental Experimental Procedures).

## SUPPLEMENTAL INFORMATION

Supplemental Information includes Supplemental Experimental Procedures, six figures, and two movies and can be found with this article online at http://dx.doi.org/10.1016/j.celrep.2015.02.010.

## AUTHOR CONTRIBUTIONS

P.X. and A.-K.H. conceived the project and designed the experiments. P.X. generated the *Nanog:H2B-GFP* mouse line and performed ESC and fixed embryo imaging experiments. M.K. performed time-lapse embryo imaging experiments. A.P. and S.D.T. carried out quantitative analyses of experimental data sets. P.X., M.K., and A.-K.H. wrote the manuscript with input from A.P. and S.D.T.

## ACKNOWLEDGMENTS

We thank X. Lou for developing the algorithm used to calculate regression curves for fluorescence intensity normalizations; J. Nichols for the *Nanog*$^{\beta\text{-}geo/+}$ mouse strain; A. Martinez-Arias for TNGA ESCs; S. Nowotschin, N. Saiz, and N. Schrode for discussions and comments on the manuscript; the Memorial Sloan Kettering Molecular Cytology and Rockefeller University Bio-Imaging Core Facilities for use of their instruments for live embryo imaging. Work in A.-K.H's. laboratory is supported by the NIH (R01-HD052115 and R01-DK084391) and NYSTEM (N13G-236). S.D.T. is supported by NIH (R00-HD074670). A.P. is supported by Finalized Research and Founding for Investments in Basic Research (RBAP11BYNP-Newton).

Received: July 14, 2014
Revised: January 4, 2015
Accepted: January 31, 2015
Published: March 5, 2015

## REFERENCES

Abranches, E., Bekman, E., and Henrique, D. (2013). Generation and characterization of a novel mouse embryonic stem cell line with a dynamic reporter of Nanog expression. PLoS ONE *8*, e59928.

Artus, J., Kang, M., Cohen-Tannoudji, M., and Hadjantonakis, A.K. (2013). PDGF signaling is required for primitive endoderm cell survival in the inner cell mass of the mouse blastocyst. Stem Cells *31*, 1932–1941.

Bessonnard, S., De Mot, L., Gonze, D., Barriol, M., Dennis, C., Goldbeter, A., Dupont, G., and Chazaud, C. (2014). Gata6, Nanog and Erk signaling control cell fate in the inner cell mass through a tristable regulatory network. Development *141*, 3637–3648.

Boroviak, T., Loos, R., Bertone, P., Smith, A., and Nichols, J. (2014). The ability of inner-cell-mass cells to self-renew as embryonic stem cells is acquired following epiblast specification. Nat. Cell Biol. *16*, 516–528.

Chambers, I., Colby, D., Robertson, M., Nichols, J., Lee, S., Tweedie, S., and Smith, A. (2003). Functional expression cloning of Nanog, a pluripotency sustaining factor in embryonic stem cells. Cell *113*, 643–655.

Chambers, I., Silva, J., Colby, D., Nichols, J., Nijmeijer, B., Robertson, M., Vrana, J., Jones, K., Grotewold, L., and Smith, A. (2007). Nanog safeguards pluripotency and mediates germline development. Nature *450*, 1230–1234.

Chazaud, C., Yamanaka, Y., Pawson, T., and Rossant, J. (2006). Early lineage segregation between epiblast and primitive endoderm in mouse blastocysts through the Grb2-MAPK pathway. Dev. Cell *10*, 615–624.

Czechanski, A., Byers, C., Greenstein, I., Schrode, N., Donahue, L.R., Hadjantonakis, A.K., and Reinholdt, L.G. (2014). Derivation and characterization of mouse embryonic stem cells from permissive and nonpermissive strains. Nat. Protoc. *9*, 559–574.

Dietrich, J.E., and Hiiragi, T. (2007). Stochastic patterning in the mouse preimplantation embryo. Development *134*, 4219–4231.

Eckersley-Maslin, M.A., Thybert, D., Bergmann, J.H., Marioni, J.C., Flicek, P., and Spector, D.L. (2014). Random monoallelic gene expression increases upon embryonic stem cell differentiation. Dev. Cell *28*, 351–365.

Faddah, D.A., Wang, H., Cheng, A.W., Katz, Y., Buganim, Y., and Jaenisch, R. (2013). Single-cell analysis reveals that expression of nanog is biallelic and equally variable as that of other pluripotency factors in mouse ESCs. Cell Stem Cell *13*, 23–29.

Filipczyk, A., Gkatzis, K., Fu, J., Hoppe, P.S., Lickert, H., Anastassiadis, K., and Schroeder, T. (2013). Biallelic expression of nanog protein in mouse embryonic stem cells. Cell Stem Cell *13*, 12–13.

Frankenberg, S., Gerbe, F., Bessonnard, S., Belville, C., Pouchin, P., Bardot, O., and Chazaud, C. (2011). Primitive endoderm differentiates via a three-step mechanism involving Nanog and RTK signaling. Dev. Cell *21*, 1005–1013.

Gendrel, A.V., Attia, M., Chen, C.J., Diabangouaya, P., Servant, N., Barillot, E., and Heard, E. (2014). Developmental dynamics and disease potential of random monoallelic gene expression. Dev. Cell *28*, 366–380.

Grabarek, J.B., Zyzyńska, K., Saiz, N., Piliszek, A., Frankenberg, S., Nichols, J., Hadjantonakis, A.K., and Plusa, B. (2012). Differential plasticity of epiblast and primitive endoderm precursors within the ICM of the early mouse embryo. Development *139*, 129–139.

Guo, G., Huss, M., Tong, G.Q., Wang, C., Li Sun, L., Clarke, N.D., and Robson, P. (2010). Resolution of cell fate decisions revealed by single-cell gene expression analysis from zygote to blastocyst. Dev. Cell *18*, 675–685.

Hatano, S.Y., Tada, M., Kimura, H., Yamaguchi, S., Kono, T., Nakano, T., Suemori, H., Nakatsuji, N., and Tada, T. (2005). Pluripotential competence of cells associated with Nanog activity. Mech. Dev. *122*, 67–79.

Kalmar, T., Lim, C., Hayward, P., Muñoz-Descalzo, S., Nichols, J., Garcia-Ojalvo, J., and Martinez Arias, A. (2009). Regulated fluctuations in nanog expression mediate cell fate decisions in embryonic stem cells. PLoS Biol. *7*, e1000149.

Kang, M., Piliszek, A., Artus, J., and Hadjantonakis, A.K. (2013). FGF4 is required for lineage restriction and salt-and-pepper distribution of primitive endoderm factors but not their initial expression in the mouse. Development *140*, 267–279.

Kurimoto, K., Yabuta, Y., Ohinata, Y., Ono, Y., Uno, K.D., Yamada, R.G., Ueda, H.R., and Saitou, M. (2006). An improved single-cell cDNA amplification method for efficient high-density oligonucleotide microarray analysis. Nucleic Acids Res. *34*, e42.

Lou, X., Kang, M., Xenopoulos, P., Muñoz-Descalzo, S., and Hadjantonakis, A.K. (2014). A rapid and efficient 2D/3D nuclear segmentation method for analysis of early mouse embryo and stem cell image data. Stem Cell Reports *2*, 382–397.

MacArthur, B.D., Sevilla, A., Lenz, M., Müller, F.J., Schuldt, B.M., Schuppert, A.A., Ridden, S.J., Stumpf, P.S., Fidalgo, M., Ma'ayan, A., et al. (2012). Nanog-dependent feedback loops regulate murine embryonic stem cell heterogeneity. Nat. Cell Biol. *14*, 1139–1147.

Messerschmidt, D.M., and Kemler, R. (2010). Nanog is required for primitive endoderm formation through a non-cell autonomous mechanism. Dev. Biol. *344*, 129–137.

Mitsui, K., Tokuzawa, Y., Itoh, H., Segawa, K., Murakami, M., Takahashi, K., Maruyama, M., Maeda, M., and Yamanaka, S. (2003). The homeoprotein Nanog is required for maintenance of pluripotency in mouse epiblast and ES cells. Cell *113*, 631–642.

Morgani, S.M., Canham, M.A., Nichols, J., Sharov, A.A., Migueles, R.P., Ko, M.S., and Brickman, J.M. (2013). Totipotent embryonic stem cells arise in ground-state culture conditions. Cell Rep. *3*, 1945–1957.

Muñoz Descalzo, S., Rué, P., Garcia-Ojalvo, J., and Martinez Arias, A. (2012). Correlations between the levels of Oct4 and Nanog as a signature for naïve pluripotency in mouse embryonic stem cells. Stem Cells *30*, 2683–2691.

Navarro, P., Festuccia, N., Colby, D., Gagliardi, A., Mullin, N.P., Zhang, W., Karwacki-Neisius, V., Osorno, R., Kelly, D., Robertson, M., and Chambers, I. (2012). OCT4/SOX2-independent Nanog autorepression modulates heterogeneous Nanog gene expression in mouse ES cells. EMBO J. *31*, 4547–4562.

Nichols, J., and Smith, A. (2012). Pluripotency in the embryo and in culture. Cold Spring Harb. Perspect. Biol. *4*, a008128.

Nichols, J., Silva, J., Roode, M., and Smith, A. (2009). Suppression of Erk signalling promotes ground state pluripotency in the mouse embryo. Development *136*, 3215–3222.

Ohnishi, Y., Huber, W., Tsumura, A., Kang, M., Xenopoulos, P., Kurimoto, K., Oleś, A.K., Araúzo-Bravo, M.J., Saitou, M., Hadjantonakis, A.K., and Hiiragi, T. (2014). Cell-to-cell expression variability followed by signal reinforcement progressively segregates early mouse lineages. Nat. Cell Biol. *16*, 27–37.

Okita, K., Ichisaka, T., and Yamanaka, S. (2007). Generation of germline-competent induced pluripotent stem cells. Nature *448*, 313–317.

Plusa, B., Piliszek, A., Frankenberg, S., Artus, J., and Hadjantonakis, A.K. (2008). Distinct sequential cell behaviours direct primitive endoderm formation in the mouse blastocyst. Development *135*, 3081–3091.

Schrode, N., Xenopoulos, P., Piliszek, A., Frankenberg, S., Plusa, B., and Hadjantonakis, A.K. (2013). Anatomy of a blastocyst: cell behaviors driving cell fate choice and morphogenesis in the early mouse embryo. Genesis *51*, 219–233.

Schrode, N., Saiz, N., Di Talia, S., and Hadjantonakis, A.K. (2014). GATA6 levels modulate primitive endoderm cell fate choice and timing in the mouse blastocyst. Dev. Cell *29*, 454–467.

Smith, A. (2013). Nanog heterogeneity: tilting at windmills? Cell Stem Cell *13*, 6–7.

Takahashi, K., and Yamanaka, S. (2006). Induction of pluripotent stem cells from mouse embryonic and adult fibroblast cultures by defined factors. Cell *126*, 663–676.

Tan, F.E., and Elowitz, M.B. (2014). Brf1 posttranscriptionally regulates pluripotency and differentiation responses downstream of Erk MAP kinase. Proc. Natl. Acad. Sci. USA *111*, E1740–E1748.

Torres-Padilla, M.E., and Chambers, I. (2014). Transcription factor heterogeneity in pluripotent stem cells: a stochastic advantage. Development *141*, 2173–2181.

Xenopoulos, P., Kang, M., and Hadjantonakis, A.K. (2012). Cell lineage allocation within the inner cell mass of the mouse blastocyst. Results Probl. Cell Differ. *55*, 185–202.

Yamanaka, Y., Lanner, F., and Rossant, J. (2010). FGF signal-dependent segregation of primitive endoderm and epiblast in the mouse blastocyst. Development *137*, 715–724.

Ying, Q.L., Wray, J., Nichols, J., Batlle-Morera, L., Doble, B., Woodgett, J., Cohen, P., and Smith, A. (2008). The ground state of embryonic stem cell self-renewal. Nature *453*, 519–523.

**Cell Reports**

**Supplemental Information**

# Heterogeneities in Nanog Expression Drive Stable Commitment to Pluripotency in the Mouse Blastocyst

**Panagiotis Xenopoulos, Minjung Kang, Alberto Puliafito, Stefano Di Talia, and Anna-Katerina Hadjantonakis**

## SUPPLEMENTAL FIGURES

**Figure S1 (related to Figure 1).**

**Comparison of *Nanog* reporter activities and NANOG expression in early blastocysts.**

(A) Schematic of FACS analyses (B-C) for the *Nanog:GFP*$^{Tg/+}$, *Nanog:H2B-GFP*$^{Tg/+}$, *Nanog:H2B-Venus*$^{Tg/+}$ and the *Nanog*$^{GFP}$ targeted (TNGA) ESCs propagated after several passages in the absence of MEFs. Numbers in FACS histograms indicate percentages of GFP- (left) and GFP+ (right) populations. R1 ESCs (red histograms) were used as negative controls for calibration of GFP- and GFP+ gates. (D) Comparison of reporter activity in *Nanog:H2B-GFP*$^{Tg/+}$ESCs grown in standard serum+LIF (top panel) and 2i+LIF conditions (bottom panel). ESCs were imaged in the same imaging session with the same imaging parameters. Colonies in 2i+LIF conditions displayed markedly

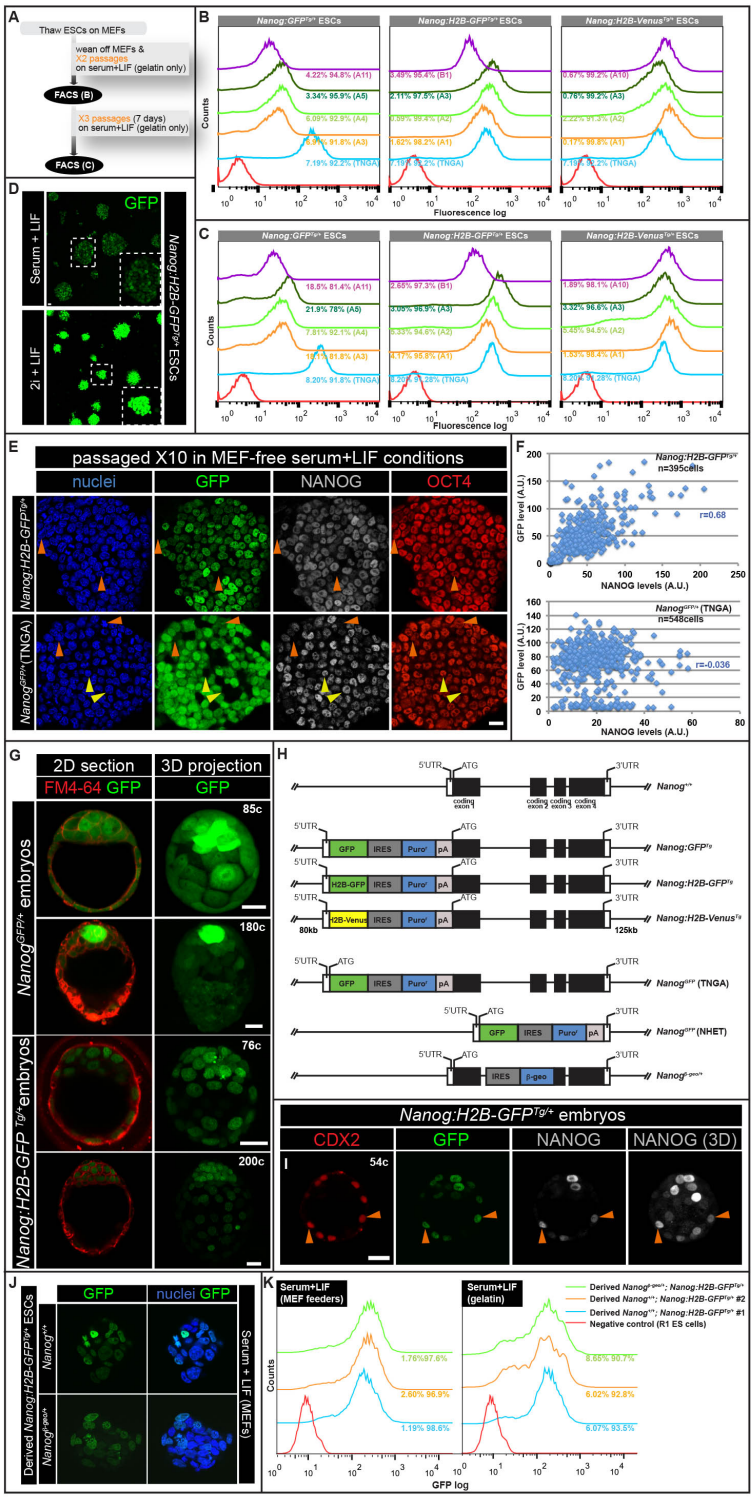


**Xenopoulos *et al.*, Supplementary Figure 1 (related to Figure 1).**

increased reporter activity and had a prominent round morphology, indicative of the ground state of self-renewal (Ying et al., 2008). (E) Immunostained *Nanog:H2B-GFP*$^{Tg/+}$ and TNGA ESCs after 10 passages in MEF-free serum+LIF conditions, stained for Hoechst, NANOG and OCT4. (F) Quantitative immunofluorescence after automated nuclear segmentation. Approximately 5 ESC colonies were used for the analysis, with one colony shown (E). GFP (y-axis) and NANOG (x-axis) fluorescence values plotted for individual ESCs. Cells displaying low levels of GFP, and NANOG observed within the population highlighted with orange arrowheads. In TNGA ESCs some NANOG+ GFP- cells were observed within colonies (yellow arrowheads). (G) Reporter activity in *Nanog*$^{GFP/+}$ and *Nanog:H2B-GFP*$^{Tg/+}$ blastocysts observed in live mid (~64-100 cells) and implanting (>150 cells) blastocysts stained with the membrane vital dye FM4-64. Reporter activity was elevated within the ICM. Reporter-expressing TE cells were observed in both strains. It should be noted that increased (4X) 488nm Ar laser power was used for imaging *Nanog*$^{GFP/+}$ blastocysts, due to dim reporter expression compared to *Nanog:H2B-GFP* embryos. Cell counting was carried out by staining with Hoechst for nuclear labeling. (H) Schematic of the endogenous *Nanog* locus, including the start of coding sequence (ATG), 4 coding exons, 5' and 3' UTRs. BAC-based transcriptional reporters were constructed by targeting GFP-IRES-Puro$^{r}$-SV40pA, H2B-GFP-IRES-Puro$^{r}$-SV40pA and H2B-Venus-IRES-Puro$^{r}$-SV40pA cassettes into the 5'UTR of the *Nanog* locus, 19bp upstream of the beginning of the ORF. The TNGA targeted allele was generated by inserting a GFP-IRES-Puro$^{r}$-pA cassette at the *Nanog* START (AUG) codon (Chambers et al., 2007). The *Nanog*$^{GFP/+}$ targeted allele was generated by replacing the ORF with a GFP-IRES-Puro$^{r}$-pA cassette (Hatano et al., 2005). The *Nanog*$^{\beta\text{-}geo/+}$ targeted allele was generated by replacing exon 2 with an IRES-β-geo cassette (Mitsui et al., 2003). (I) Immunofluorescence images of an early (54 cells) *Nanog:H2B-GFP*$^{Tg/+}$ blastocyst stained for NANOG and the TE marker CDX2. Reporter and NANOG protein expression were noted in TE cells (orange arrowheads). (J-K). Imaging and FACS analysis of embryo derived *Nanog:H2B-GFP*$^{Tg/+}$ ; *Nanog*$^{+/+}$ and *Nanog:H2B-GFP*$^{Tg/+}$ ; *Nanog*$^{\beta\text{-}geo/+}$ ESCs. ESCs were stained with Hoechst for nuclei labeling. Numbers in FACS histograms indicate percentages of GFP- (left) and GFP+ (right) populations. *r*=Pearson correlation coefficient. Scale bar: 20μm.

**Figure S2 (related to Figure 2).**

***Nanog:H2B-GFP* BAC transgene marks segregating EPI cells in mid blastocysts.**

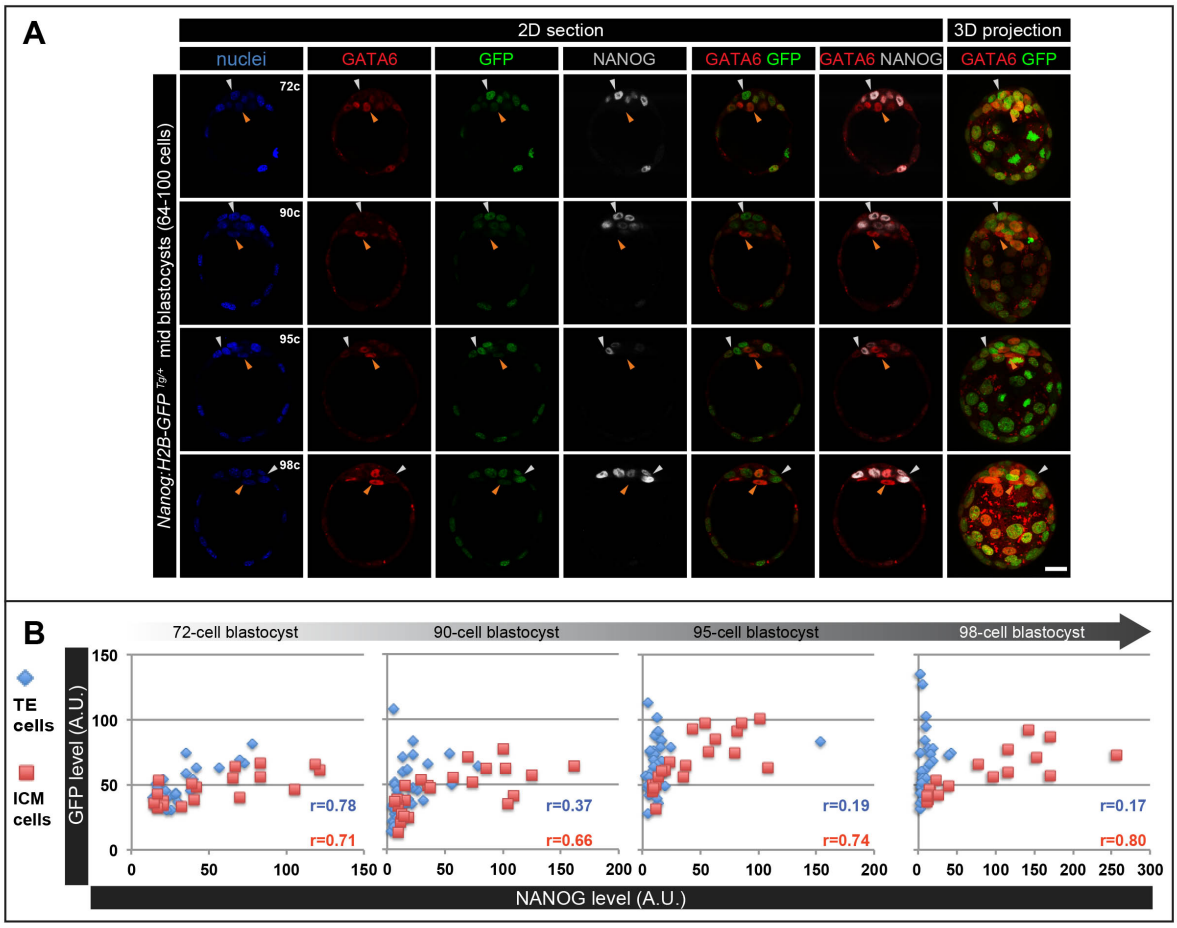


**Xenopoulos *et al.*, Supplementary Figure 2 (related to Figure 2).**

*Nanog:H2B-GFP* reporter expression in mid-blastocyst stage (~64-100 cell) embryos counterstained with Hoechst, anti-GATA6 and NANOG antibodies. (A) Embryos were imaged similarly to those in **Figure 2B**, albeit in a different imaging session and with different imaging parameters. White arrowheads identify segregating EPI-progenitors, orange arrowheads identify PrE-progenitors. (B) Quantitative immunofluorescence after MINS automated nuclear segmentation and fluorescence intensity normalization of the embryos shown in (A). Analysis was performed as in **Figure 2C**. All embryos shown were imaged with the same parameters. *R* = Pearson correlation coefficient. Scale bar: 20μm.

**Figure S3 (related to Figure 3).**

**Modulation of FGF signaling alters *Nanog* expression distributions within the ICM.**

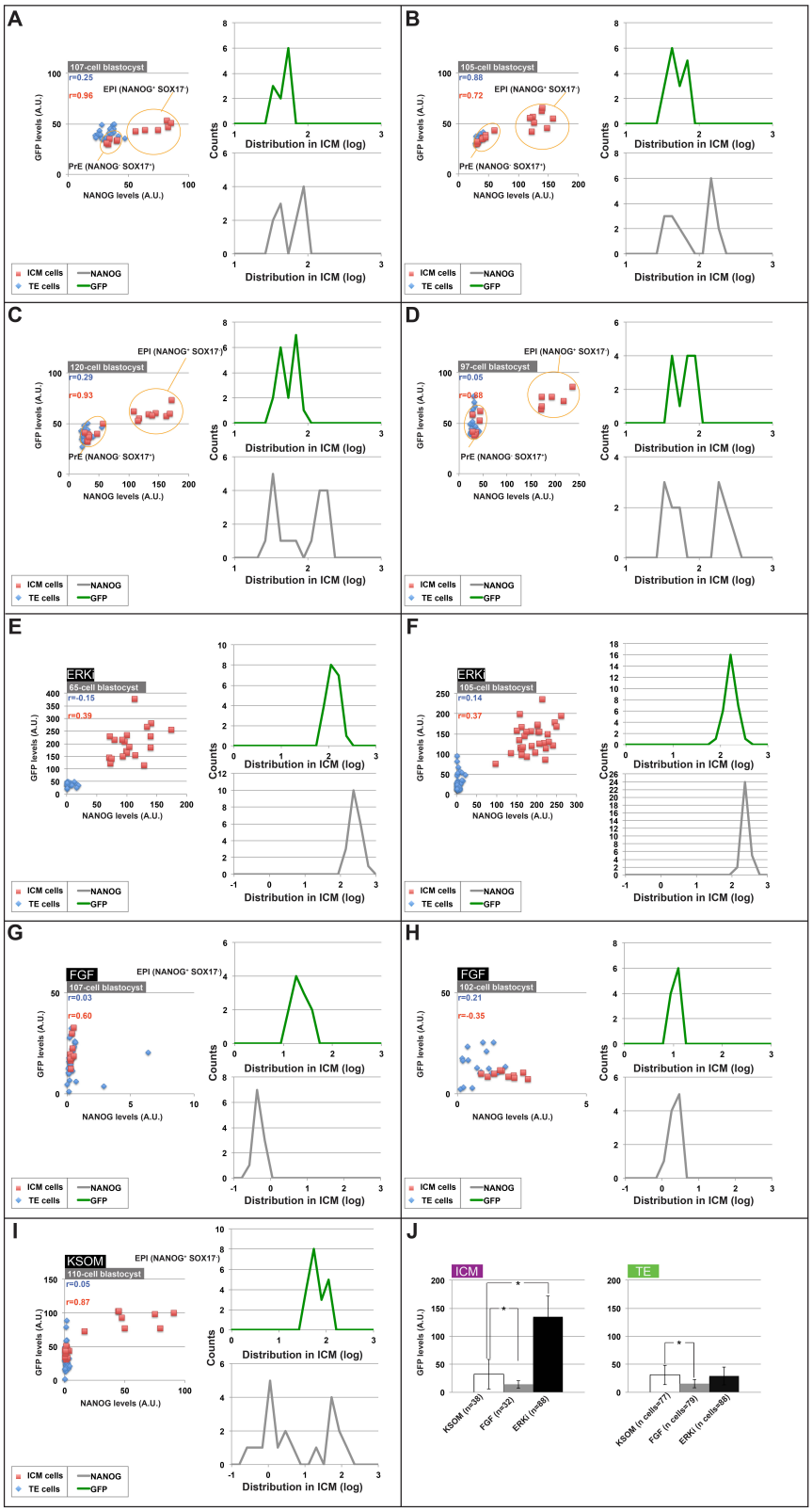


**Xenopoulos *et al.*, Supplementary Figure 3 (related to Figure 3).**

(A-D) Reporter and NANOG expression analyses in late (>100 cell) *Nanog:H2B-GFP*$^{Tg/+}$ blastocysts counterstained with Hoechst, anti-SOX17 and NANOG antibodies. After MINS automated nuclear segmentation, analyses were performed as shown in **Figure 3A**. Embryos in (A-B) were imaged in the same imaging session as the embryo in **Figure 3A**. Embryos in (C-D) were imaged in a different imaging session and with different imaging parameters. (E-I) Reporter and NANOG expression analyses in cultured embryos (in control KSOM medium, or medium supplemented with exogenous FGF or the ERK1/2 inhibitor PD0325901), which were imaged within the same imaging session and with

the same imaging parameters as in **Figure 3B** (all cultured embryos belonged in the same litter). After automated nuclear segmentation, analysis was performed similarly as in **Figure 3C**. Note that the x- and y-axis scales of scatter plots are different due to changes in reporter and NANOG expression in cohorts of cultured embryos. In (J) mean values for the GFP channel for ICM or TE cells were pooled from the KSOM (n=2), FGF (n=3) or ERKi (n=3) treated embryos. Error bars indicate s.d. *r* = Pearson correlation coefficient. Asterisks indicate significant differences (*P*, <0.05 by the *t* test).

**Figure S4 (related to Figure 4).**

**Reporter activity is not diluted in dividing cells and lineage preference in the mother cell is inherited by daughter cells.**

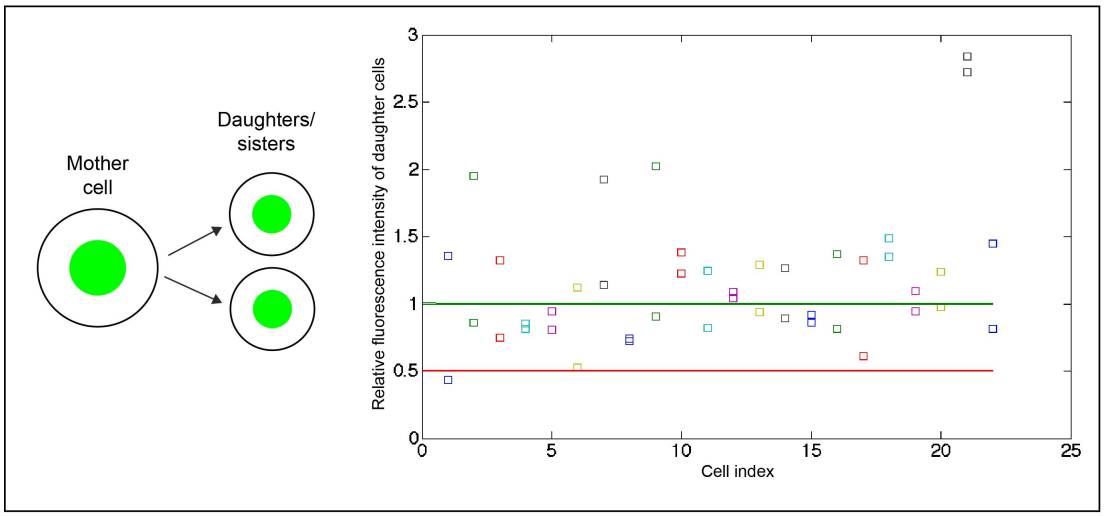


**Xenopoulos *et al.*, Supplementary Figure 4 (related to Figure 4).**

(A) GFP is not diluted after cell proliferation. We considered dividing EPI cells and for each track we plotted the mean fluorescence intensity value for the hour preceding, and the hour following, mitosis. We excluded bursts in fluorescence intensity due to chromosome condensation. We obtained 3 intensity values referring to mother and two daughter (i.e. sister) cells (depicted in the cartoon on the left) and plotted the relative intensity of the sisters (i.e. sister intensity/mother intensity) per each cell division (depicted on the right panel). Red and green colored continuous lines represent values of 0.5 (perfect dilution, each sister inherits one half of the total protein present in the mother cell), 1 (perfect compensation, each sister inherits the value of the mother), respectively. The average total fluorescence of sister cells slightly exceed 1 (1.16), indicating that daughter cells reached approximately the same level of fluorescence intensity as their mother cell.

**Figure S5 (related to Figure 5).**

**Reporter expression is decreased upon exogenous FGF2 treatment, when all ICM cells commit toward the PrE lineage.**

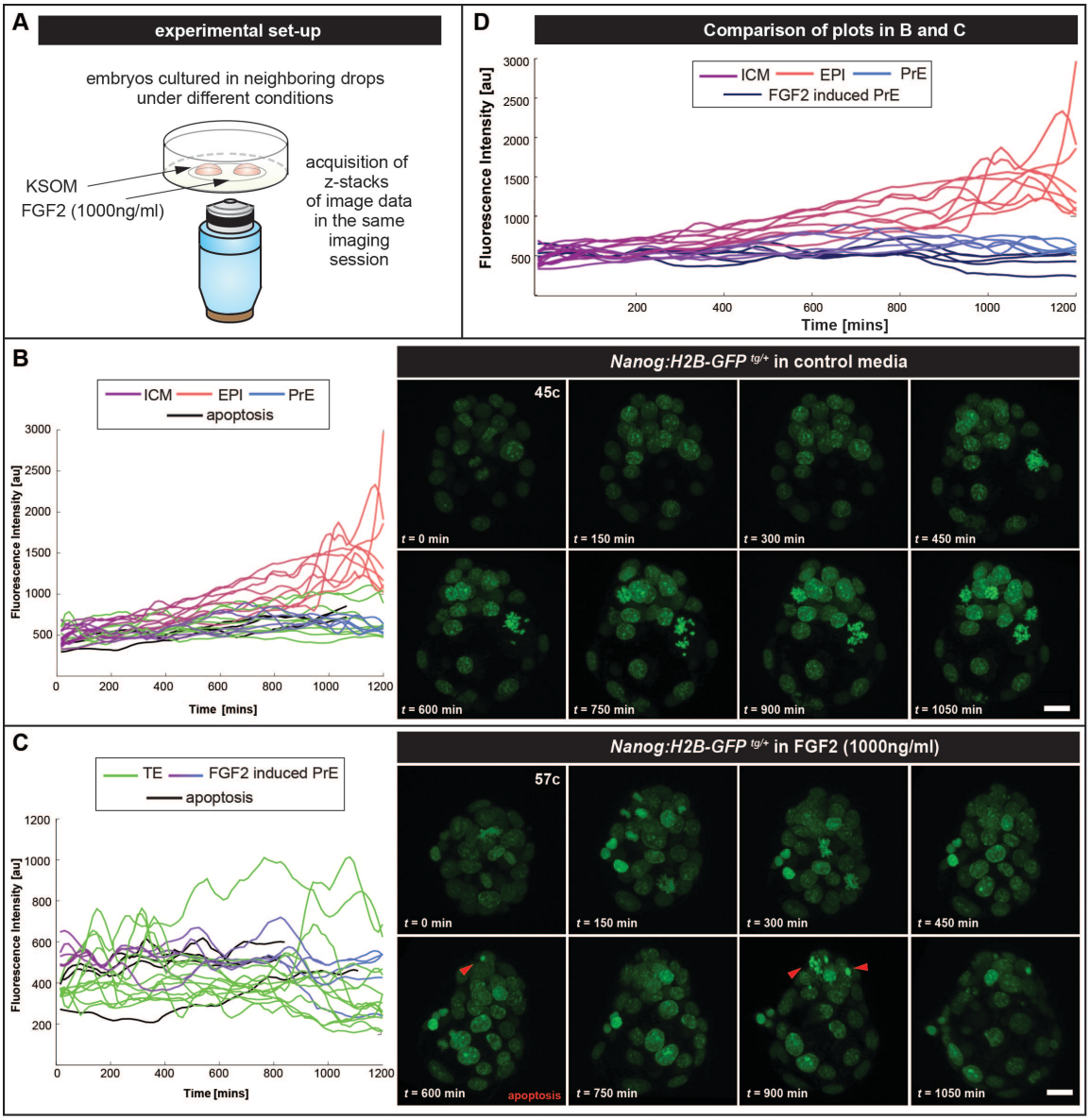


**Xenopoulos *et al.*, Supplementary Figure 5 (related to Figure 5).**

(A) Schematic of 3D time-lapse live imaging experiment design. Embryos cultured in different media conditions were imaged in the same session. Representative *Nanog:H2B-GFP* $^{tg/+}$ blastocysts recovered at E3.5 (comprising 45-cells, 57-cells at start of experiment/movie) and cultured *ex utero* for 1200 minutes in (B) KSOM (control media) or (C) FGF2 (1000ng/ml). Left

panels, quantification of GFP fluorescence values over time. Right panels, single time-points from 3D time-lapse movies. In control media, individual ICM cells committed to either EPI or PrE lineages, and consequently exhibited increased or decreased *Nanog:H2B-GFP* reporter activity, respectively. Under conditions of FGF treatment, all ICM cells adopted a PrE identity and exhibited a decrease in reporter activity. (D) Superimposed plot of GFP quantifications from time-lapse movies in (B) and (C) revealing decreased levels of GFP intensity in embryo cultured in the presence of FGF.

**Figure S6 (related to Figure 5).**

**Quantitative analysis of *Nanog:H2B-GFP* reporter using cycloheximide and FGF2 suggested that half-life of H2B-GFP is less than 6 hours.**

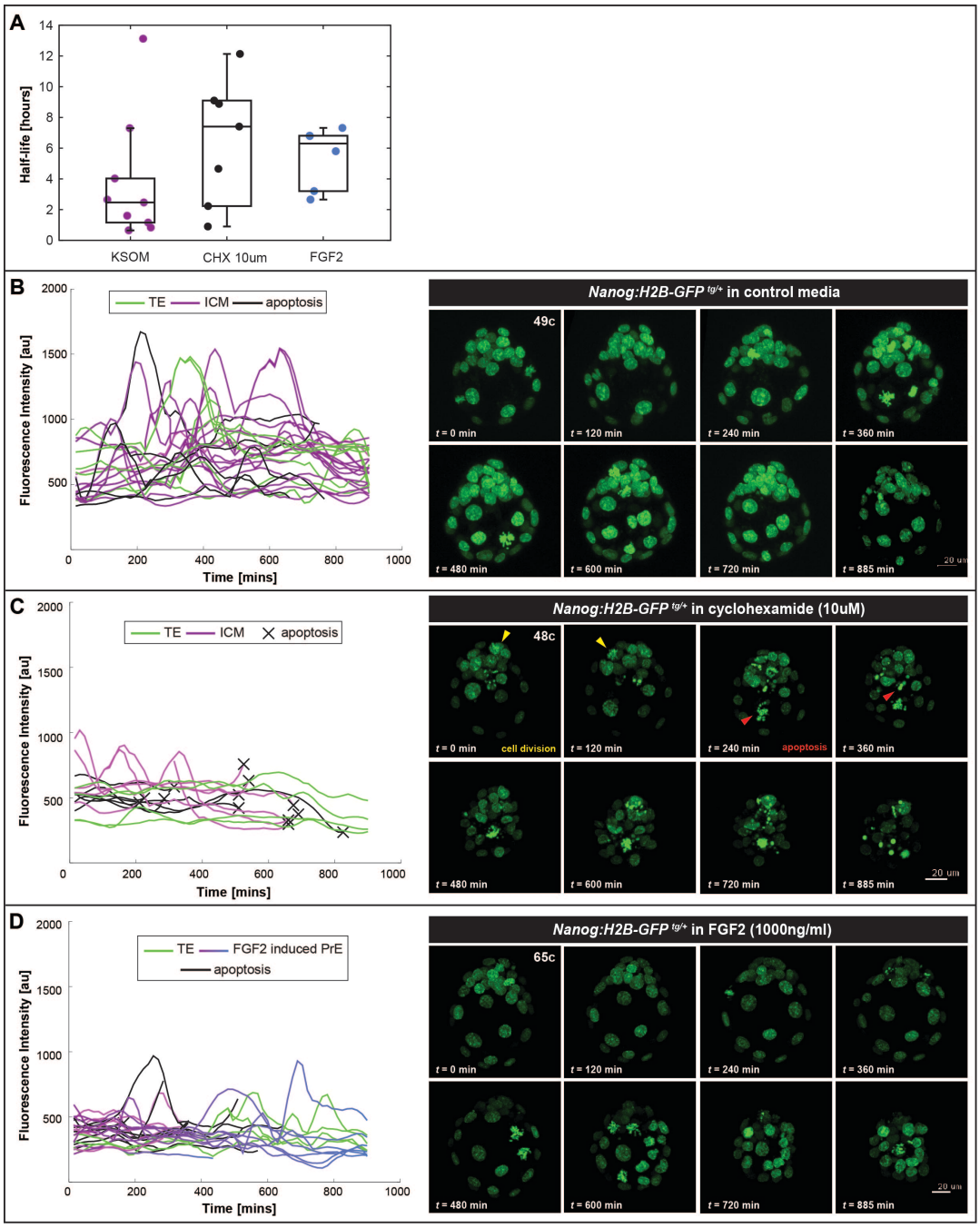


**Xenopoulos *et al.*, Supplementary Figure 6 (related to Figure 5).**

(A) Box plots showing the average time of half-life calculated from individual cells from 3D time-lapse movies of *Nanog:H2B-GFP* embryos in different culture conditions of (B) KSOM (control media), (C) cycloheximide (CHX, 10μM) or (D) FGF2 (1000ng/ml). Embryos cultured in different media conditions were imaged in the same session. From the movie of embryo in KSOM, only PrE cells were counted for the calculation of H2B-GFP half-life, since only those cells exhibit downregulation of reporter activity. From the movies of embryos in CHX or FGF2 treatments, both EPI and PrE-biased cells had taken into account for the calculation of H2B-GFP half-life. The mean decay rate of PrE cells from the embryo in KSOM is T = 3.8 ± 4.0 (h). The results from CHX and FGF2 treatment are T= 6.5±4.0 (h) and 5.4±2.0 (h), respectively. The higher decay rates in the condition of CHX or FGF2 are possibly due to the initial high level of fluorescence intensity in EPI-biased cells. (B-D) Quantification of GFP fluorescence values and images of single time-points from a time-lapse of *Nanog:H2B-GFP*$^{Tg/+}$ blastocysts recovered at E3.5 (comprising 49-cells, 48-cells and 65-cells at start of experiment/movie) and cultured *ex utero* in different conditions for 900 minutes. (C) Under conditions of CHX treatment, the embryo had few incidences of cell divisions, suggesting that the treatment had partially worked (yellow arrowhead). However, by the end of the movie, most of cells underwent apoptosis (red arrowhead).

## SUPPLEMENTAL MOVIES

**Movie S1 (related to Figures 4 and 5). Changes in GFP-positive cell distribution within the ICM of *Nanog:H2B-GFP*$^{Tg/+}$ embryos from mid to late blastocyst stages.**

(A-C) 3D time-lapse movies of 3D reconstructed images of *Nanog:H2B-GFP*$^{Tg/+}$ blastocysts. (A) Embryo was collected around E3.5 (~50 cells) and cultured *ex utero* thereafter. Image data was acquired with the Zeiss LSM780 confocal system. At the end of the movie, GFP-hi cells had formed the EPI lineage, whereas GFP-low cells formed the epithelial PrE layer on the surface of the ICM. Reporter expression in the TE cells diminishes as the blastocyst develops. The embryo depicted in **Figure 4** can be seen in this movie. (B) Embryo was collected around E3.5 (54 cells) and cultured *ex utero* thereafter. Image data was acquired with the Zeiss 510 confocal system. Tracked nuclei are highlighted by dots; the outline of each dot depicts the lineage choice. Cells highlighted in red-color outlined dots are EPI progenitor cells; cells highlighted with the blue-color outlined dots are PrE progenitor cells. Movie depicts embryo in **Figure 5A**. (C) Embryo was collected around E3.75 (83 cells) and cultured *ex utero* thereafter. Image data was acquired with the Zeiss LSM510 confocal system. Tracked nuclei are highlighted as in (B). Movie depicts embryo in **Figure 5C**. For all movies, the z-section interval was 2μm and the embryos were imaged every 15min. Red arrowheads points to events of apoptosis and yellow arrowheads mark events of cell division.

**Movie S2 (related to Figure 6). Changes in GFP-positive cell distribution within the ICM of a *Nanog:H2B-GFP*$^{Tg/+}$ embryo treated with an ERK inhibitor.**

3D time-lapse movie of 3D reconstructed images of a *Nanog:H2B-GFP*$^{Tg/+}$ blastocyst collected around E3.5 (48-cells at start of experiment/movie) and cultured *ex utero* in the presence of the ERK inhibitor PD0325901. z-section interval was 2μm and time interval was 15min. At the end of the movie, the majority of the ICM consisted of GFP-hi cells that had acquired an EPI identity. Yellow arrowheads mark cell divisions in EPI-specified cells. Movie depicts embryo in **Figure 6**.

## SUPPLEMENTAL RESULTS

**Extracting *Nanog* transcriptional dynamics from *Nanog:H2B-GFP* reporter.** To study the dynamics of *Nanog* transcription, we used a reporter construct in which the promoter of *Nanog* drives expression of H2B-GFP. This construct has the advantage of providing information on *Nanog* transcription as well as allowing single cell resolution and tracking. In this Section, we use a computational approach to estimate how the dynamics of H2B-GFP relates to the dynamics of *Nanog* transcription.

(i) *H2B-GFP dilution*. Cell proliferation demands that an increasing number of H2B molecules are incorporated in nuclei. Depending on the amount of free H2B molecules in the cytoplasm, cell division could cause a dilution of histone molecules. We found that $NANOG^+$ EPI cells proliferate significantly more than $NANOG^-$ PrE cells, suggesting that the dilution of H2B-GFP does not contribute significantly to the observed differentiation dynamics. To further verify whether we could detect a dilution of H2B-GFP signal we focused on dividing EPI cells. We found no evidence for dilution of H2B-GFP (**Figure S4**). Collectively, our observations imply that H2B dilution does not affect our measurements of *Nanog* transcriptional dynamics.

(ii) *H2B-GFP half-life*. Histones can be long-lived molecules. It is, therefore, important to understand how the lifetime of H2B-GFP might affect the measurements of *Nanog* transcriptional dynamics in the pre-implantation embryo. To this end, we first estimated experimentally an upper bound for the half-life of H2B-GFP, using three independent approaches. First, we treated embryos with cycloheximide (to inhibit protein translation) and measured the decay of H2B-GFP (**Figure S6**). High concentrations of cycloheximide are toxic and causes massive and rapid cell death in embryos. We, therefore, used a relatively low concentration (10$\mu$M), which causes a partial inhibition of protein translation, as exemplified by the fact that we still observe cell divisions, which require protein translation. Estimating a half-life of H2B-GFP using an exponential decay fit, therefore, gives us an upper bound on the half-life of H2B-GFP. We find such upper bound to be 6.5±4 hours. We also repeated similar analysis for embryos treated with FGF4 (**Figure S5**). In such embryos, all cells assume the PrE fate and downregulated *Nanog* expression. From the measurements of the decay of H2B-GFP, we obtain an upper bound for H2B-GFP half-life of 5.4±2 hours, compatible with the estimate from

the cycloheximide experiment (**Figure S6**). Finally, we use the decay of the fluorescence traces from PrE cells, in which a clear and sharp decrease of H2B-GFP fluorescence is observed at the onset of cell differentiation (**Figure S6**). Assuming that the production of NANOG rapidly switch from an on to an off state at the time of differentiation, we can fit the decay of the fluorescence signal with an exponential decay and extrapolate an upper bound for H2B-GFP. Performing this analysis on several cells provides the value 3.8±4 hours. Collectively, these experiments allow us to conclude that the half-life of H2B-GFP is shorter than 6 hours and, in fact, not very dissimilar for NANOG half-life, which is about 4 hours (Abranches et al., 2013).

To determine which changes in *Nanog* transcription can be effectively tracked with a reporter of half-life of few hours, we used a mathematical model that describes the dynamics of H2B-GFP:

$ds/dt=a(t)-s/t-s/t_1$

$ds^*/dt=s/t-s^*/t_1$

where a(t) is H2B-GFP production rate, s is the amount of immature H2B-GFP, s* is the amount of fluorescent H2B-GFP, t is the maturation rate of GFP and $t_1$ is the lifetime of H2B-GFP. Estimate of t suggest that it is of the order of 30 minutes, implying that GFP maturation is much faster than the timescales of interest. We, therefore, assume that s is always close to steady state. The equations above reduce to:

$ds^*/dt=b(t)-s^*/t_1$

where $b(t)=a(t)t_1/(t+t_1)$.

Next, we needed to estimate the amount of noise in the detection of *Nanog:H2B-GFP* reporter activity. To this end, we performed filtering on the traces of non-dividing EPI traces to remove small (time) scale fluctuations but keep slow dynamics. Filtering was achieved by smoothing on the scale of 2.5h. Noise was then estimated by calculating the mean deviation of the original signal from the filtered signal. We obtained an estimate of about 6% of average *Nanog* expression levels in EPI cells. Assuming that we can reliably measure changes in gene expression that are above two-fold of the level of noise, we conclude that changes in gene expression which are two-folds or higher and persists for at least 2 hours can be reliably tracked. Collectively, this analysis shows that our transcriptional reporter allows us to follow the transcriptional dynamics of *Nanog* in pre-implantation embryos with temporal resolution of less than 2 hours. Such resolution is sufficient for our studies of cell differentiation dynamics, which happens on much longer timescales (10-15 hours) (Leveau and Lindow, 2001).

## SUPPLEMENTAL EXPERIMENTAL PROCEDURES

**Generation of reporter constructs by BAC modification**.

BAC clone RP23-117I23 (CHORI, BACPAC Resources) containing the *Nanog* gene, was modified using RED/ET recombination [GeneBridges; (Angrand et al., 1999)] as described previously (Okita et al., 2007). Reporter cassettes were generated by ligating GFP-IRES-Puro$^r$, H2B-GFP-IRES-Puro$^r$ and H2B-Venus-IRES-Puro$^r$ fragments with a PGK-Hygro-FRT cassette (GeneBridges). The *Nanog* 5'UTR was targeted (19bp upstream of the beginning of the ORF) by attaching homology arms to both ends of reporter cassettes by PCR amplification using the following 50bp oligos: NanogGFP-Fw (5'-TTTGCATTAGACATTTAACTCTTCTTTCTATGATCTTTCCTTCTAGACACGCCACCATGGTGAGCAAGGGCGAG-3'), NanogH2B-Fw (5'- (5'-TTTGCATTAGACATTTAACTCTTCTTTCTATGATCTTTCCTTCTAGACACGCCACCATGCCAGAGCCAGCG-3') and NanogpIRESpuro3-R (5'-GCGAGGGAAGGGATTTCTGAAAAGGTTTTAGGCAACAACCAAAAAACTCACGCCAAGCTCTAGCTAGAGGTCGACG-3'). The underlined sequences depict the homology arms for the *Nanog* 5'UTR, which are the same as used previously (Okita et al., 2007).

**Generation of transgenic mESCs and mice**.

Transgenic mESCs were generated by nucleofection (Amaxa, Lonza) of R1 ESCs (Nagy et al., 1993) with 10μg of undigested modified BAC DNA purified with the large-construct kit (Qiagen). After 4 days 1.5μg/ml puromycin selection was started. Resistant colonies were picked after 10 days of selection. Clonal lines were expanded and propagated in the presence or absence of mouse embryonic fibroblasts (MEFs). At least two ESC clones for each reporter were analyzed. Transgenic mice were generated by pronuclear injection of undigested modified BAC carrying the *Nanog:H2B-GFP* cassette purified with the large-construct kit (Qiagen). The BAC construct was injected into F1XF1 zygotes by the Memorial Sloan Kettering Mouse Genetics Core Facility following standard protocols (Nagy, 2003.). Founder animals were identified by PCR. Amplification generated a 475bp fragment from the GFP cassette using primers IMR872 Fw: AAGTTCATCTGCACCACCG and IMR873 Rev: TGCTCAGGTAGTGGTTGTCG. Four transgenic founder lines, #32, #38, #40 and #105, were established each exhibiting a similar pattern and level of reporter expression. Only one line (#38) is presented here in detail. The

transgene exhibited Mendelian inheritance, stable transgene activity and comparable levels of reporter expression within litters and across generations. Animals homozygous for the transgene were viable and fertile; only embryos heterozygous for the transgene were characterized in this study. Mice were maintained in accordance with National Institute of Health guidelines for the care and use of laboratory animals and under the approval of the MSKCC Institutional Animal Care and Use Committee.

**Embryo collection and *in vitro* culture.**

Embryos were recovered in M2 (Millipore) and cultured in KSOM (Millipore) medium as described previously (Kang et al., 2013). For FGF incubation experiments, FGF2 (R&D systems) at concentrations of 1000 ng/mL, supplemented with 1 μg/mL heparin (Sigma) was added to KSOM medium. For incubation experiments with an ERK1/2 inhibitor and cycloheximide, 1μM PD0325901 (StemGent) and 10μM cycloheximide (Sigma-Aldrich) were added to KSOM medium. Staining of live embryos with the vital dye FM4-64 (Invitrogen), was carried out as described previously (Plusa et al., 2008). Late morulae (~16-32 cell embryos) with or without zona pellucidae were cultured in micro-drops (10 embryos/15 μL drop) under mineral oil for 36 hours.

**ESC culture.**

Cell lines used in this study were *Nanog:GFP*$^{Tg/+}$, *Nanog:H2B-GFP*$^{Tg/+}$ and *Nanog:H2B-Venus*$^{Tg/+}$ transgenic R1 ESCs, targeted *Nanog*$^{GFP/+}$-clone A ESCs (TNGA) (Chambers et al., 2007) and embryo derived *Nanog:H2B-GFP*$^{Tg/+}$ ; *Nanog*$^{+/+}$ or *Nanog:H2B-GFP*$^{Tg/+}$ ; *Nanog*$^{tm1-geo/+}$ ESCs. ESCs were thawed on mouse embryonic fibroblast (MEF) feeder layers in medium containing high glucose Dulbecco's modified Eagle's medium (D-MEM, Gibco) supplemented with 15% fetal bovine serum (FBS), 0.1 mM 2-mercaptoethanol, 1 mM non-essential amino acids, 1 mM sodium pyruvate, 2 mM glutamine, 100 units/mL penicillin and 100 μg/mL streptomycin and recombinant leukemia inhibitory factor (LIF). ESCs were propagated routinely on gelatin in the absence of feeders. ESCs were cultured on gelatin in 2i (ESGRO, Millipore, supplemented with 1μM PD0325901 and 3μM Chiron, StemGent) and LIF.

**FACS analysis and cell sorting.**

ESCs were prepared for FACS analysis and sorting using a FACSCalibur (BD Biosciences) and MoFlo (Dako) high-speed cell sorter and analyzer respectively by harvesting cells in 0.025% trypsin/EDTA (Invitrogen) followed by neutralization of trypsin in growth medium. Live single cell populations were selected for further analyses based on Forward Scatter (FSC) and Side Scatter (SSC) characteristics, as well cell viability evaluations using Propidium Iodide (PI) staining. Parental R1 ESCs were used as a negative non-fluorescent control (Nagy et al., 1993). Cells with fluorescence levels (GFP, H2B-GFP or H2B-Venus) within this range were considered to be negative. Histograms of the FACS data were generated using FlowJo (Tree Star, Inc).

**ESC cell derivation from embryos.**

ESCs were derived from *Nanog:H2B-GFP*$^{Tg/+}$ ; *Nanog*$^{+/+}$ or *Nanog:H2B-GFP*$^{Tg/+}$ ; *Nanog*$^{tm1-geo/+}$ blastocysts as described previously (Czechanski et al., 2014). Newly derived ESC lines were gradually weaned off 2i, and propagated in standard serum + LIF conditions in the presence or absence of MEFs.

**Image data acquisition and processing.**

512 X 512 pixel images were acquired on Zeiss LSM510 META or LSM700 laser scanning confocal microscopes. Fluorescence was excited with a 405-nm laser diode (Hoechst), a 488-nm Argon laser (GFP), a 543-nm HeNe laser (Alexa-Fluor-543/555) and a 633-nm HeNe laser (Alexa-Fluor-633/647 or FM4-64). Images were acquired using a 40X objective, with optical section thickness of 0.5μm for ESCs and 1μm for embryos. Raw data were processed using ZEN software (Carl Zeiss Microsystems). For any given experiment, all ESC and embryo images were obtained with the same image acquisition parameters (laser intensity, gain, pinhole size).

**Fluorescence Intensity Normalization using Robust Curve Fitting**

Assuming that the true intensities of the Hoechst channel are consistent throughout the depth of view, we used a robust curve fitting technique to model the intensity attenuation as a function of the depth *Z* (see **Figure 2A**). Specifically, we used a generalized logistic function as the underlying model because the observed data points exhibited a strong S shape. The fitting

process serves the purpose of model parameter estimation. In particular, it optimizes the sum of squared loss between observed points and their estimates using unconstrained nonlinear optimization. In MATLAB, unconstrained nonlinear optimization can be implemented using the function 'fminsearch'. However, two issues may cause the fitting result problematic. Firstly, 'fminsearch' is prone to local minimum because of the non-convexity of the objective function. Also, outlier data points may severely deteriorate the fitting result. To overcome these issues we incorporated two additional techniques. Firstly, we used multiple randomized initializations. Secondly, we applied the RANdom SAmple Consensus (RANSAC) algorithm to make curve fitting robust towards outliers.

**Cell tracking**

To track cells even in the presence of extensive drift, either of cohorts of cells within the embryo or of the entire embryo, we used PIV tracking (Raffel, 1998). For each plane of a given segmented cell this algorithm seeks the best match in the next frame in terms of cross correlation between successive fluorescence images. The median over the planes is then taken as the cell index in the next frame. Among the untracked cells, around 20-30% of cells were dividing or undergoing apoptosis and were manually tracked, while for others their fluorescence signal was unclear as they were at the very top or bottom of the z-stack, or were incorrectly segmented. To correct for whole-embryo drift we calculated the embryo's center of mass and subtracted the motion of the embryo from the individual cell trajectories. Fluorescence signal was corrected for changes in penetration along axial position. The intensity profile along the z direction of all segmented nuclei was fitted with a linear function, and the obtained correction factor was used to correct fluorescence intensities at each time point. Time traces of fluorescence intensities were filtered using Savitzky-Golay polynomial fitting with order 3 and length 7 (i.e. around 50 minutes forward and backward). Of note, an increase in fluorescence emitted from the *Nanog:H2B-GFP* transgene was routinely observed during mitosis, due to chromosome condensation; the resulting rapid oscillations in reporter activity were not considered to be caused by changes in gene expression. Tracking scripts were written in MATLAB (http://katlab-tools.org/). Data were numerically analyzed with the open source software package GNU Octave.

## SUPPLEMENTAL REFERENCES

Abranches, E., Bekman, E., and Henrique, D. (2013). Generation and characterization of a novel mouse embryonic stem cell line with a dynamic reporter of Nanog expression. PLoS One *8*, e59928.

Angrand, P.O., Daigle, N., van der Hoeven, F., Scholer, H.R., and Stewart, A.F. (1999). Simplified generation of targeting constructs using ET recombination. Nucleic acids research *27*, e16.

Chambers, I., Silva, J., Colby, D., Nichols, J., Nijmeijer, B., Robertson, M., Vrana, J., Jones, K., Grotewold, L., and Smith, A. (2007). Nanog safeguards pluripotency and mediates germline development. Nature *450*, 1230-1234.

Czechanski, A., Byers, C., Greenstein, I., Schrode, N., Donahue, L.R., Hadjantonakis, A.K., and Reinholdt, L.G. (2014). Derivation and characterization of mouse embryonic stem cells from permissive and nonpermissive strains. Nat Protoc *9*, 559-574.

Hatano, S.Y., Tada, M., Kimura, H., Yamaguchi, S., Kono, T., Nakano, T., Suemori, H., Nakatsuji, N., and Tada, T. (2005). Pluripotential competence of cells associated with Nanog activity. Mech Dev *122*, 67-79.

Kang, M., Piliszek, A., Artus, J., and Hadjantonakis, A.K. (2013). FGF4 is required for lineage restriction and salt-and-pepper distribution of primitive endoderm factors but not their initial expression in the mouse. Development *140*, 267-279.

Leveau, J.H., and Lindow, S.E. (2001). Predictive and interpretive simulation of green fluorescent protein expression in reporter bacteria. J Bacteriol *183*, 6752-6762.

Mitsui, K., Tokuzawa, Y., Itoh, H., Segawa, K., Murakami, M., Takahashi, K., Maruyama, M., Maeda, M., and Yamanaka, S. (2003). The homeoprotein Nanog is required for maintenance of pluripotency in mouse epiblast and ES cells. Cell *113*, 631-642.

Nagy, A., Gertsenstein, M., Vintersten, K., and Behringer, R. (2003.). Manipulating the mouse embryo: a laboratory manual. Cold Spring Harbor Laboratory Press, Cold Spring Harbor, New York.

Nagy, A., Rossant, J., Nagy, R., Abramow-Newerly, W., and Roder, J.C. (1993). Derivation of completely cell culture-derived mice from early-passage embryonic stem cells. Proc Natl Acad Sci U S A *90*, 8424-8428.

Okita, K., Ichisaka, T., and Yamanaka, S. (2007). Generation of germline-competent induced pluripotent stem cells. Nature *448*, 313-317.

Plusa, B., Piliszek, A., Frankenberg, S., Artus, J., and Hadjantonakis, A.K. (2008). Distinct sequential cell behaviours direct primitive endoderm formation in the mouse blastocyst. Development *135*, 3081-3091.

Raffel, M., Willert, C.E., and Kompenhans, J. (1998). Particle Image Velocimetry: A Practical Guide. Springer, Berlin.

Ying, Q.L., Wray, J., Nichols, J., Batlle-Morera, L., Doble, B., Woodgett, J., Cohen, P., and Smith, A. (2008). The ground state of embryonic stem cell self-renewal. Nature *453*, 519-523.